Rose G. Long
Icahn School of Medicine at Mount Sinai,
Leni and Peter W. May Department of Orthopaedics,
New York, NY 10029;
Collaborative Research Partner Annulus Fibrosus Rupture Program of AO Foundation,
Davos 7270, Switzerland
e-mail: rose.long@mssm.edu

Olivia M. Torre
Icahn School of Medicine at Mount Sinai,
Leni and Peter W. May Department of Orthopaedics,
One Gustave Levy Place, Box 1188,
New York, NY 10029
e-mail: olivia.torre@icahn.mssm.edu

Warren W. Hom
Icahn School of Medicine at Mount Sinai,
Leni and Peter W. May Department of Orthopaedics,
One Gustave Levy Place, Box 1188,
New York, NY 10029
e-mail: warren.hom@mssm.edu

Dylan J. Assael
Icahn School of Medicine at Mount Sinai,
Leni and Peter W. May Department of Orthopaedics,
One Gustave Levy Place, Box 1188,
New York, NY 10029
e-mail: dylan.assael@icahn.mssm.edu

James C. Iatridis[1]
Icahn School of Medicine at Mount Sinai,
Leni and Peter W. May Department of Orthopaedics,
One Gustave Levy Place, Box 1188,
New York, NY 10029;
Collaborative Research Partner Annulus Fibrosus Rupture Program of AO Foundation,
Davos 7270, Switzerland
e-mail: james.iatridis@mssm.edu

Design Requirements for Annulus Fibrosus Repair: Review of Forces, Displacements, and Material Properties of the Intervertebral Disk and a Summary of Candidate Hydrogels for Repair

There is currently a lack of clinically available solutions to restore functionality to the intervertebral disk (IVD) following herniation injury to the annulus fibrosus (AF). Microdiscectomy is a commonly performed surgical procedure to alleviate pain caused by herniation; however, AF defects remain and can lead to accelerated degeneration and painful conditions. Currently available AF closure techniques do not restore mechanical functionality or promote tissue regeneration, and have risk of reherniation. This review determined quantitative design requirements for AF repair materials and summarized currently available hydrogels capable of meeting these design requirements by using a series of systematic PubMed database searches to yield 1500+ papers that were screened and analyzed for relevance to human lumbar in vivo measurements, motion segment behaviors, and tissue level properties. We propose a testing paradigm involving screening tests as well as more involved in situ and in vivo validation tests to efficiently identify promising biomaterials for AF repair. We suggest that successful materials must have high adhesion strength (~0.2 MPa), match as many AF material properties as possible (e.g., approximately 1 MPa, 0. 3 MPa, and 30 MPa for compressive, shear, and tensile moduli, respectively), and have high tensile failure strain (~65%) to advance to in situ and in vivo validation tests. While many biomaterials exist for AF repair, few undergo extensive mechanical characterization. A few hydrogels show promise for AF repair since they can match at least one material property of the AF while also adhering to AF tissue and are capable of easy implantation during surgical procedures to warrant additional optimization and validation. [DOI: 10.1115/1.4032353]

1 Introduction

Lower back pain is the leading cause of global disability [1,2] and is commonly associated with IVD herniation, where nucleus pulposus (NP) tissues extrude through defects in the AF resulting in back pain, leg numbness, and weakness. Discectomy or microdiscectomy procedures are a well-indicated intervention for radicular pain resulting from herniation and are the surgical standard of care with improved outcomes compared to nonoperative management [3–6]. Discectomy removes the offending herniation tissue but does not repair the remaining annular defect or restore IVD function. The lack of effective AF closure techniques results in a 5–25% rate of complications involving reherniation or recurrent pain at the same level [7–9]. Unrepaired AF defects result in altered tissue and motion segment biomechanics and can also lead to accelerated IVD degeneration [10–14]. Disruptions to the AF can also result in detrimental nerve and vascular ingrowth [15], which are implicated in discogenic back pain [16]. There remains a need for clinical solutions to repair AF defects.

Currently available procedures for AF closure are designed to prevent reherniation and do not restore mechanical functionality or promote repair of the injured AF. Suture techniques were unable to restore IVD intradiscal pressures in animal models [17]. More recently improved and simplified suturing techniques for AF closure (e.g., Xclose, Anulex Technologies, Inc., Minnetonka, MN) do not significantly reduce reherniation rates [18]. AF implants such as the Barricaid® (Intrinsic Therapeutics, Woburn, MA) prevented NP tissue reherniation [19,20] and reduced facet joint pressure [21]. However, neither this promising device nor sutures restored mechanical behaviors of the motion segment or promoted tissue regeneration so long-term follow-up results will be important to assess. Tissue engineering strategies offer promise for cell and drug delivery to promote tissue repair and may also be able to address the needs of preventing herniation and restoring motion segment mechanical behavior.

[1]Corresponding author.
Manuscript received August 26, 2015; final manuscript received December 8, 2015; published online January 27, 2016. Editor: Beth A. Winkelstein.

Many experimental tissue engineered hydrogels have been investigated to repair damaged AF because they can be modified to act as sealants, adhesives, and scaffolds by modifying the large variety of biomaterial, composition, and structural forms that are available.

This review informs tissue engineering of the human AF by addressing three objectives: (1) to review reported values for intradiscal pressures, strains in the IVD of the human spine, and material properties of the AF in order to develop quantitative design criteria for modulus, strain at failure, and adhesive strength for hydrogels for AF repair; (2) to summarize currently available hydrogels and assess their potential based on these criteria; and (3) to outline a testing paradigm for AF repair strategies. Several important reviews on IVD tissue engineering and AF repair exist [12,22–26]. Nerurkar et al. provided an important review on design criteria for IVD tissue engineering [26], yet several recent papers exist and there lacks a clear consensus on the quantitative design criteria for AF repair, and these design criteria are necessary for optimizing biomaterials for successful AF repair. We use some of the design objectives for AF repair recently proposed by Likhitpanichkul et al. including strong adhesion to native tissue and biomechanically tuned to match AF mechanical properties [27]. This work focuses on AF repair using hydrogels that may be implemented to augment discectomy procedures and does not describe NP replacement, or whole tissue engineered IVDs, which are more appropriate solutions for advanced degenerative disk disease in place of fusion or total disk arthroplasty.

2 Literature Review Methods

PubMed was used as the database for this review with multiple primary searches (Table 1). Keywords for searches focused on identifying papers relevant to four main topics concerning the human lumbar spine: intradiscal pressure and in vivo spine biomechanics; human motion segment behaviors; human AF material properties; and hydrogels for AF repair. A total of 1519 articles were identified. We included papers with human subjects and human tissues, and papers directly related to the topics of in vivo spine biomechanics, in situ spine biomechanics, AF material properties, and hydrogels for AF repair. Additional references were included when identified from manuscripts found in the review, including papers beyond the date range of the inclusion criteria. The in vivo spine biomechanics literature was reviewed with a focus on in vivo human lumbar strain and ranges of motion (ROM) measurements, which we considered to be particularly important for characterizing AF repair design criteria. The in situ motion segment literature was reviewed for human lumbar motion segment stiffness values, which we considered target values for restoration of IVD biomechanics upon repair. It is important to acknowledge that a larger range for these values exists across humans and is also available from the many excellent papers on in vitro and animal IVD biomechanics not included in this review and also that a safety factor should be considered. All nonEnglish articles were excluded except for intradiscal pressure measurements and hydrogels. This review included 99 articles.

3 In Vivo and In Situ Spine Biomechanics

3.1 Intradiscal Pressure. Quinnell et al. measured 40 IVDs and found intradiscal pressures ranged 0.06–0.24 MPa with an average of 0.15 MPa while lying prone [28], which were smaller than the previously recorded values of 0.38 MPa [29] (Fig. 1). Wilke et al. and Sato et al. reported pressures of 0.11 MPa ($n = 1$) and 0.09 MPa ($n = 8$) while prone, respectively [30,31] that were closer to Quinnell et al. Intradiscal pressures were greater in standing and sitting positions than prone with few exceptions [30–33]. Ten studies measured sitting pressures with averages ranging from 0.32 MPa [32] to 1.18 MPa [34] and with sample sizes ranging from 1–18 [28–33,35–38]. Eight studies reported standing pressures with averages ranging from 0.27 MPa [32] to 0.88 MPa [34] and sample sizes ranging from 1–7 [28–34,39]. Average pressures were greater for sitting than for standing, perhaps because in sitting, 100% of the load is transmitted through the IVD versus 85% in standing [40]. Sitting has only slightly greater intradiscal pressure than standing, suggesting that any increase may be associated with bending and muscle recruitment rather than total pressure on the IVD [41].

The measured pressures vary between subjects and studies, as seen by the range of maximum and minimum values indicated by error bars (Fig. 1). The greatest systematic change in the measured intradiscal pressure values was a decrease following a change in sensor technology to a piezoresistive diaphragm syringe around 1970. Nachemson's early work used a pressure gauge on a polyethylene tubing coupled with an electromanometer [34–36,42]. Quinnell et al. measured the pressure of the disk by measuring fluid at equilibrium with the NP [28]. In 1970, Nachemson introduced the piezoresistive strain gauge between a diaphragm and a pressure transducer [29]. The piezoresistive sensor allowed for dynamic measurements and a greater range of measurements. In 1999, Wilke et al. published long-term (24 hrs) pressure measurement using a telemeterized implanted pressure sensor [30], and Sato et al. recorded measurements using a side mounted gauge membrane transducer [31]. Intradiscal pressure measurements from degenerated IVDs are lower than from healthy IVDs [31,33,43].

To determine AF repair design criteria, data for all compiled papers on intradiscal pressure were used to calculate sample-size weighted averages of intradiscal pressures in prone, sitting, and standing postures, with mean values of 0.22 MPa, 0.75 MPa, and 0.59 MPa and maximal pressures values of 0.41 MPa [29], 1.50 MPa [34], and 1.07 MPa [34], respectively. AF repair materials must withstand the prone pressure immediately postsurgery when the patient is recovering from anesthesia and must withstand the sitting and standing pressures shortly following surgery as the patient returns to normal activities. The repair must withstand higher intradiscal pressures associated with more rigorous activities. To be more conservative with design criteria, values for degenerated IVDs were excluded from the weighted-average calculations (since average degenerated IVD intradiscal pressures are lower), which also targets repairing IVDs to a healthy state.

3.2 In Vivo Spine Biomechanics. In vivo ROM measurements of human lumbar IVDs can be used, with measured strains, to estimate the strains an AF repair must withstand. ROM of 6–13 deg, 1–5 deg, 2.9–11 deg and 2–3 deg in flexion, extension, lateral bending, and torsion, respectively, have been reported [44,45] (Table 2). When the whole spine is moved from a 20 deg extension to a 60 deg flexion posture, L2/3, L3/4, and L4/5 IVDs experience the largest ROM of approximately 9 deg, and L1/2 and L5/S1 experiences 7 deg and 6 deg, respectively [46,47].

Strains induced by spinal segment motions in vivo were measured directly using MRI and fluoroscopic X-ray techniques to visualize the displacement of the vertebral bodies adjacent to the disk during flexion, extension, and lateral bending movements. The posterior AF has been reported to experience tensile strains as high as 50–65% in tension when moving from a standing to fully flexed position [48] (Table 2). In 1995, Kanayama et al. found large local strains of up to 90% in the posterior AF, but those were calculated using an FEA model and measured displacements in flexion, so were excluded [49]. Due to the anatomy of lumbar IVDs, the posterior region has a smaller IVD height and a large ROM compared to the anterior portion, resulting in large apparent strains as measured using radiography. When moving from an upright or extended position to a flexed position, the posterior AF experiences larger strains (65% tensile strain in L4/5) compared to the anterior AF (29% compressive strain in L4/5) [47]. In situ testing (Supplemental Table 1 is available under the "Supplemental Data" tab for this paper on the ASME Digital Collection [58]) also indicated that complex intradiscal

Table 1 PubMed search terms, inclusion criteria, and the number of articles found and used

Section	Search terms	No. of articles	Inclusion criteria	No. of articles used from initial search
Intradiscal pressure	Pressure human IVD in vivo	66	Human	12
	lumbar human intradiscal pressure in vivo	29	In vivo studies	0
In vivo spine biomechanics	AF strain	91	English language	4
	Disc strain in vivo	86	Human	5
	Disk kinematics in vivo	284	ROM and strains from in vivo studies	7
In situ motion segment stiffness	IVD mechanics	273	English language	18
	IVD stiffness	440	Human Stiffness and apparent modulus from lumbar motion segments.	14
AF material properties	Human AF mechanical properties	61	English language	6
	Human AF modulus	30	Human AF tissue	3
	Human AF material properties	31	Published 2009 or later	0
	Human AF modulus OR tensile OR compressive OR shear	228		2
AF repair hydrogels	Hydrogel AND IVD	136	English language	5
	AF repair	104	Relevant AF repair material	10
	(Hydrogel OR scaffold OR sealant OR biomaterial) NOT repair AND AF	75	Biomechanical testing performed Published 2007 or later	13
		1556	Total number of articles	99

deformations and strain patterns occur within the IVD with strain rates varying from 1.66%/deg to −0.94/deg in the posterior AF from compression and torsion, respectively [59]. At the tissue level, strains are distributed in complex motions and are therefore of lower values than measured radiographically from vertebra to vertebra motions. Nevertheless, multiple papers validate high values of posterior AF strain and we conclude that an AF repair should have high strains to avoid risk of failure. An AF repair hydrogel should be designed to have tensile failure strain exceeding 65%.

Disk height and depth, measured from X-ray and magnetic resonance images, varies from 4 to 6 mm posteriorly and 30 to 34 mm between different levels of the spine (minimum values correspond to L1/2 and L5/S1, respectively) (Table 2) [50,51]. Dimensions of the IVD are useful for informing the required volume for an AF repair biomaterial, for example, a 5 mm square

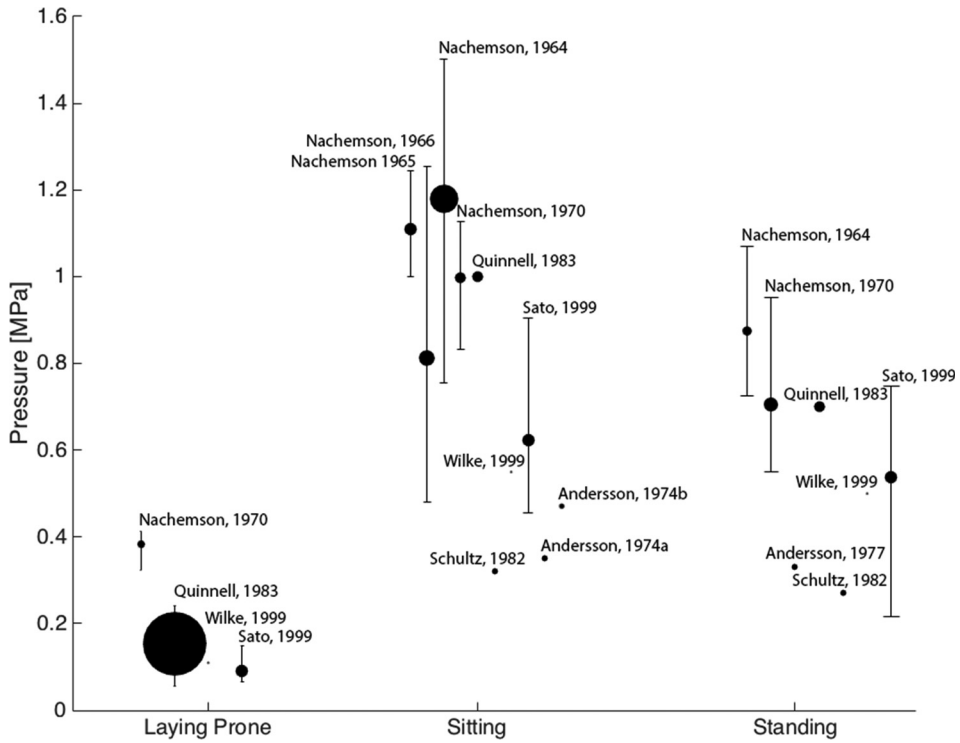

Fig. 1 Intradiscal pressure increases on average 3.4 and 2.7 times in sitting and standing postures from lying prone (0.223 MPa), respectively. Marker size indicates number of samples in each study with Wilke having one and Quinnell having forty. Label indicates first author and publication year of study. Error bars indicate the total range of values found in the study. Range data not available for studies indicated by markers without error bars. Values from Refs. [29] and [33–36] were multiplied by 0.0981 to convert from kg/cm^2 to MPa. [28–39].

defect the depth of an average human annulus would require about 125 mL. The deep posterior AF thickness, ranging from 2.5 to 5 mm, also affects gelation kinetics and hence is important for establishing feasibility of UV-activated or light sensitive biomaterials where the required depth of light penetration is a constraint [50]. Anterior IVD height ranges from 8 mm at L1/2 to 14 mm at L4/5 [50,51]. Although there is limited variability between lumbar levels of an individual spine, there are notable differences between individuals as evidenced by a wide range of measurements acquired from 41 different L4/5 disks with recorded values of 30.4 ± 4.5 mm [50].

3.3 In Situ Motion Segment Stiffness. IVD axial stiffness values range 0.44–2.42 kN/mm and can be as high as 5.1 kN/mm under relatively fast dynamic loading conditions [60–63] (Table 3). The posterior and anterior shear stiffness of the IVD are 0.47 kN/mm and 0.58 kN/mm, respectively, when exposed to a 250 N shear force [64]. Torsional stiffness has been measured at 3.18 ± 0.89 N m/deg at 6 deg of axial rotation at 0.5 Hz cyclic loading [65]. In lateral bending, the stiffness ranges 4.21–10.04 N m/deg [66]. Although axial stiffness may not be significantly altered by discectomy [61], it is a parameter that serves as a measure of the stiffness an AF repair must restore once it becomes integrated with the surrounding native AF.

4 AF Material Properties

The AF is a laminated angle-ply composite structure with layers oriented at ∼±30 deg angles in the outer AF and ∼±45 deg in the inner AF [89], resulting in heterogeneous and highly anistotropic mechanical properties. Furthermore, the AF is highly hydrated, varying in composition with region, and the constituent proteins interact under loading to induce nonlinear and viscoelastic behaviors. AF material properties exhibit viscoelastic and nonlinear material behaviors that are also sensitive to orientation (axial, circumferential, or radial), structure (single lamella or multilamellae), degree of hydration, and tissue location (anterior, posterolateral, inner, or outer). AF tissue material properties are summarized based on these criteria and separated by mode of testing (Table 4).

4.1 Tension. Under physiological loading, the AF is subjected to circumferential tensile hoop stresses that resist the highly pressurized NP. The linear circumferential tensile modulus ranges 11–29 MPa in the posterolateral region, which is the region most relevant to AF repair [90–92] (Fig. 2). Nonlinearities in AF material behaviors can result in variability of 10 × or more, and O'Connell et al. found tensile modulus in the circumferential direction 2.7 MPa in the toe region and 20.9 in the linear region. The range of circumferential tensile modulus of posterolateral, outer AF is approximately an order of magnitude larger than the axial (0.42–0.82 MPa) and radial (0.21–0.45 MPa) moduli (Table 4) [91–93]. AF tissue is stiffer at the outer AF regions as compared to the interior AF regions with values of 13 MPa and 4.8 MPa, respectively [94]. The structure of the AF allows the

Table 2 In vivo geometry and strain of human lumbar IVDs

		L1/2	L2/3	L3/4	L4/5	L5/S1	Reference
Anterior–posterior disk length		34 mm	34 mm	33 mm	30.4 ± 4.5 mm 33 mm	30.0 ± 4.4 mm 31 mm	Zhong et al. [50] Pearcy and Tibrewal [51]
Disk height	AAF	8 mm	11 mm	12.5 mm	14 mm	13 mm	Pearcy and Tibrewal [51]
	PAF	4 mm	4.5 mm	4.5 mm	10.27 ± 2.28 mm 5.5 mm 6.07 ± 1.97	4.5 mm	Miao et al. [53] Pearcy and Tibrewal [51] Miao et al. [53]
Max Flex ROM		7 ± 4 deg	9.2 ± 3.9 deg 12.99 deg	9.5 ± 4.4 deg 6.1 ± 1.5 deg 10.91 deg	9.3 ± 5.4 deg 9.0 ± 2.1 deg 12.69 deg	6.3 ± 5.4 deg 7.3 ± 1.1 deg 10.33 deg	Lee et al. [46] Nagel et al. [47] Aiyangar et al. [52]
		8 ± 5 deg	10 ± 2 deg	PAF: $X = 3.6 \pm 1.6$ mm, $Y = 4.1 \pm 1.2$ mm, 12 ± 1 deg	PAF: $X = 4.5 \pm 1.2$ mm, $Y = 5.4 \pm 1.0$ mm, 13 ± 4 deg	PAF: $X = 1.1 \pm 0.9$ mm, $Y = 4.2 \pm 1.1$ mm, 9 ± 6 deg	Pearcy et al. [44] and Kanayama et al. [49]
		9.4 deg	9.2 deg	10.3 deg	9.5 deg	9.5 deg	Stokes [54]
Max Ext. ROM				PAF: $X = 0.6$ ± 0.6 mm, $Y = 0.1 \pm 0.8$ mm	PAF: $X = 0.1 \pm 0.2$ mm, $Y = 0.0 \pm 0.1$ mm	PAF: $X = 2.6 \pm 2.6$ mm, $Y = 3.7 \pm 1.9$ mm	Kanayama et al. [49]
		5 ± 2 deg	3 ± 2 deg	1 ± 1 deg	2 ± 1 deg	5 ± 4 deg	Pearcy et al. [44]
Max lateral bending ROM			2.9 ± 2.4 deg	3.4 ± 2.1 deg	4.7 ± 2.4 deg		Li et al. [55]
Max Ext. ROM		5 ± 2 deg	3 ± 2 deg	1 ± 1 deg	2 ± 1 deg	5 ± 4 deg	Pearcy et al. [44]
Max lateral bending ROM		10 deg	2.9 ± 2.4 deg 11 deg	3.4 ± 2.1 deg 10 deg	4.7 ± 2.4 deg 6 deg	3 deg	Li et al. [55] Pearcy and Tibrewal [51]
Max torsion ROM		2 deg	3.2 ± 1.9 deg 2.5 ± 2.3 deg 2 deg	2.8 ± 1.7 deg 2.4 ± 2.6 deg 3 deg	2.9 ± 2.1 deg 3 deg	2 deg	Xia et al. [56] Li et al. [55] Pearcy and Tibrewal [45]
Strain at full flexion				AAF = −25% PAF = +50%	AAF = −29% PAF = +65%	AAF = −24% PAF = +29%	Nagel et al. [48]
			AAF = −17 ± 8% PAF = +26 ± 9% Shear 18 ± 16%	AAF = −15 ± 10% PAF = +22 ± 13% Shear 29 ± 17%			Wang et al. [57]

AAF = Anterior AF; PAF = Posterior AF; − = Compressive; + = Tensile; ROM = Range of motion.

tissue to withstand biaxial tensile strains with a modulus of 9.8–87 MPa [48,95,96].

Poisson's ratio is the negative ratio between transverse and axial strain and is dependent on orientation. The Poisson's ratio in the axial, radial, and circumferential directions are 0.61, 0.79, and 2.27, respectively [92]. These values of Poisson's ratio, which are much greater than 0.5, highlight the anisotropic nature of the AF and are not used as a design parameter.

Tensile testing of single lamellae specimens along the fiber direction results in maximal fiber recruitment and the largest tensile modulus values, ranging from 16 to 82 MPa [91,91–99]. Tensile moduli of single lamellae from the outer portions of AF tissue approximately double that from the inner portions with averages of 64.8 MPa and 31.2 MPa, respectively [92,93,98,100,112].

4.2 Compression. Compressive properties of the AF are important for distributing vertical loads as well as confining the NP. In vivo, compressive loads on the IVD result in axial compression of the AF and bulging of the NP, which radially compresses the AF. Several studies have examined the AF under confined compression, determining the parameters aggregate modulus (H_A), and hydraulic permeability (k), which is a measurement of the viscoelasticity of the tissue due to its resistance to fluid flow through the material. Aggregate modulus ranges from 0.4–3 MPa (excluding the viscoelastic measurements of 6 MPa from Freeman et al.) and permeability ranges from $2.1–5 \times 10^{-16}$ m^4/N s [101–104].

4.3 Shear. Shear properties of the AF are important for controlling and limiting motion between vertebrae during bending and twisting of the spine. The magnitude of the complex shear modulus ($|G^*|$) is the shear modulus under dynamic conditions and the phase shift angle between stress and strain (δ), and is a relative measure of viscoelasticity. The complex shear modulus has a range of 0.10–0.28 MPa and δ has a range of 9–35 deg depending on the frequency and shear strain amplitude [105].

5 Hydrogels Used for AF Repair

An ideal biomaterial for AF repair would mimic its material properties with easy application during surgical procedures to restore IVD biomechanics and promote regenerative repair without risk of herniation. Biomaterials that are substantially more rigid than the AF will herniate because local stress concentrations develop that prevent tissue integration over time [24,113]. Biomaterials with moduli that are much lower than the native IVD are unlikely to restore biomechanical behaviors of the motion segment. Developing experimental biomaterials for AF repair to meet these design objectives and match healthy, AF tissue properties remains an unmet challenge for existing AF repair hydrogels.

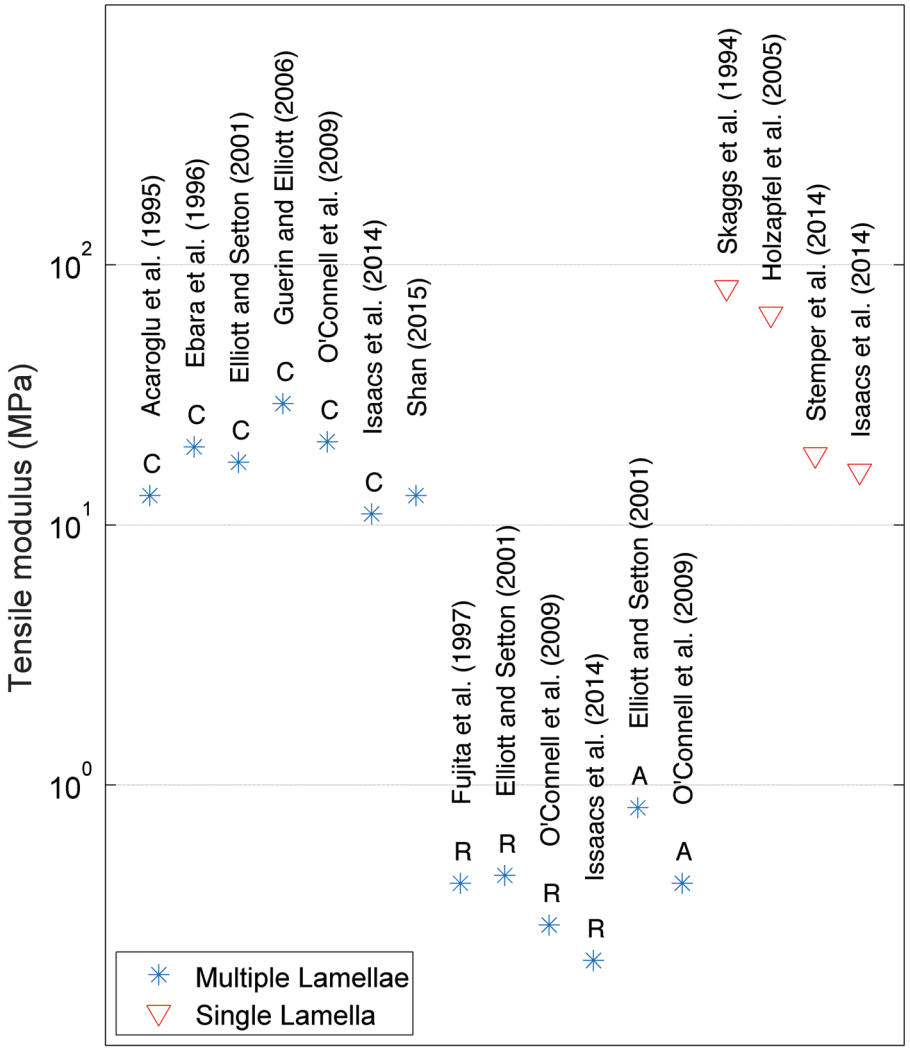

Fig. 2 Tensile moduli values reported for human AF with different orientation (C = cirumferential; R = radial; and A = axial) and for single lamella and multiple lamellae samples. Tensile moduli are reported as the linear Young's moduli values from Refs. [90–94], [97–100], [106], and [107].

While many experimental hydrogels have been developed to address AF repair following injury due to herniation or discectomy, relatively few have undergone rigorous mechanical testing to assess the biomechanical compatibility between the hydrogel and native AF tissue. These hydrogels have been evaluated for their tensile, compressive, and shear material properties as well as for their adhesive strength and gelation kinetics (Table 5).

Tensile behaviors of the AF and AF repair biomaterials are important to maintain AF tensile stresses, which are necessary to restore IVD pressurization and restrain spinal motions. This review revealed that tensile modulus is the most commonly studied mechanical parameter for experimental hydrogels for AF repair with 12 out of 19 studies using tensile modulus as an evaluation parameter.

Electrospinning is a compelling fabrication method for AF repair biomaterials due to the ability to create oriented, aligned fibers. Nerurkar et al. created a scaffold for AF repair using poly-ε-caprolactone fibers that were electrospun to create fibers of varying angles designed to mimic the AF lamellar architecture [114]. A single layer scaffold had tensile modulus of 5.8 ± 3.1 MPa after 4 weeks in culture [114], within 1 order of magnitude of AF material properties (Table 4). Fiber orientation was varied from 0 deg, 30 deg, and 90 deg, and the greatest tensile moduli values occurred in 0° oriented scaffolds [130]. This single layer structure was modified with the addition of an opposing bilayer offset at 120 deg, and improved tensile modulus to 14.2 ± 2.5 MPa [115]. Electrospun scaffolds demonstrated further improvement in tensile modulus with the addition of bovine mesenchymal stem cells and in vitro dynamic loading, which increased the tensile modulus to approximately ∼20 MPa and also improved extracellular matrix production [116,117], which closely approximates the circumferential tensile modulus of human AF tissue (Table 4).

The importance of fiber alignment for AF tissue engineered constructs was demonstrated by additional groups. The tensile moduli of poly-ε-caprolactone prepared with nonoriented and oriented fibers were 2.5 MPa and 7.25 MPa, respectively [118]. Aligned electrospun polycarbonate and polyurethane fibers were also found to have a dramatically higher tensile modulus compared to randomly oriented fibers and exhibited stable tensile modulus values after 4 weeks of culture [119,120]. Prestrain further enhanced tensile modulus in electrospun degradable polycarbonate urethane-anionic dihydroxyl oligomer scaffolds seeded with bovine AF cells [121]. Electrospun scaffolds are structural biomaterials, which do very well in matching AF structural hierarchy, tensile properties, and anisotropy, yet are not injectable and require surgical implantation.

Injectable biomaterials for AF repair have been investigated for tensile behaviors. An implantable shape memory poly(D,L-lactide-*co*-trimethylene carbonate) material can be delivered via injection through a small opening but exhibited tensile modulus of 1.7–2.5 MPa at 40 °C [122], which is substantially lower than the tensile modulus of native AF tissues (Table 4). The tensile moduli

Table 3 Human IVD motion segment stiffness and apparent modulus values

Parameter	Values	Facet joints removed	Ligaments removed	Reference
Axial stiffness	1.73 ± 0.45 kN/mm, 2 kN/mm	Yes	Yes	Beckstein et al. [62] and Marini et al. [67]
	1.17 ± 0.68 kN/mm	Yes	No	Shea et al. [61] and O'Connell et al. [68][b]
	1.4 ± 0.48 kN/mm	No	No	Landham et al. [69], Frei et al. [70], Okawa et al. [71], and McGlashen et al. [72][b]
	0.44–2.42 kN/mm	n.s.	n.s.	Nachemson et al. [60], Gardner-Morse and Stokes [63], Kiehl et al. [73],[b] and Stokes and Gardner-Morse [74]
Dynamic stiffness	5.0–30 Hz: 0.25–3.66 kN/mm	Yes	Yes	Izambert et al. [75]
	0.001–1.0 Hz: 3.51–5.14 kN/mm	Yes	No	Costi et al. [76]
	0.01–10.0 Hz: 3.24–4.15 kN/mm	No	No	Smeathers and Joanes [77]
	0.42±0.20 kN/mm	No	No	Alkalay et al. [78]
Apparent modulus[a]	2.16–10.48 MPa	No	No	Keller et al. [79]
Torsional stiffness	3.18 ± 0.89 N m/deg	Yes	Yes	Showalter et al. [65]
	2.1–2.9 N m/deg	Yes	No	Costi et al. [76] and Amin et al. [80]
	7.78–3.63 N m	No	No	Zirbel et al. [81]
	8.40 ± 1.09 N m/deg	No	No	Schmidt et al. [82]
	10–13 N m/deg	n.s.	n.s.	Stokes and Gardner-Morse [74]
	3.51±1.77 N m/deg	n.s.	n.s.	Thompson et al. [66] and Haughton et al. [83]
Flexion stiffness	2.30–3.30 N m/deg	Yes	No	Costi et al. [76] and Amin et al. [80]
	4.89–6.64 N m/deg	Yes	No	Garges et al. [84]
	0.02 kN/mm	No	No	Brown et al. [85]
	1.80–5.50 N m/deg	No	No	Schmidt et al. [82] and Miller et al. [86]
	0.07–0.36 kN/mm	n.s.	n.s.	Thompson et al. [66]
Extension stiffness	1.6–3.5 N m/deg	Yes	No	Costi et al. [76] and Amin et al. [80]
	7.21–9.09 N m/deg	Yes	No	Garges et al. [84]
	2.60–7.60 N m/deg	No	No	Schmidt et al. [82] and Miller et al. [86]
	0.19−1.02 kN/mm	n.s.	n.s.	Thompson et al. [66]
Left-right lateral bending stiffness	3.4–4.6 N m/deg	Yes	No	Costi et al. [76]
	1.11 ± 0.67 N m	No	No	Zirbel et al. [81]
	2.30–4.40 N m/deg	No	No	Schmidt et al. [82] and Miller et al. [86]
	2.90–4.30 N m/deg	n.s.	n.s.	Gardner-Morse and Stokes [74]
	4.21–10.04 N m/deg	n.s.	n.s.	Gardner-Morse and Stokes [63]
Anterior–posterior shear stiffness	0.11–0.21 kN/mm	Yes	No	Costi et al. [76] and Amin et al. [80]
	0.44–0.61 kN/mm	No	Yes	Lu et al. [64]
	0.10–0.27 kN/mm	No	No	Miller et al. [86] and Bisschop et al. [87,88]
	0.26–0.45 kN/mm	n.s.	n.s.	Stokes and Gardner-Morse [74]

[a]Calculated from three-parameter-solid model; and n.s. indicates motion segment preparation details not specified.
[b]Calculated from reported force and displacement values.

of a poly(1,8-octanediol malate) scaffold matched AF tissue tensile modulus when polymerization time was increased to 3–9 days of polymerization, with moduli ranging 15–26 MPa [131]. Thermogelling hydrogels, such as a poly(*N*-isopropylacrylamide) and chondroitin sulfate with aldehyde modified chondroitin sulfate (PNIPAAm-g-CS), are adhesive to the adjacent tissue upon injection and had tensile moduli comparable to native AF tissue [132]. These biomaterials exhibit promise for matching AF tensile modulus, and further optimization and validation are warranted, including measurement of additional material properties.

The unconfined compressive modulus of an injectable adhesive PNIPAAm-PEG/PEI was ~0.01 MPa without the addition of a gluteraldehyde crosslinker, and between 0.06–0.08 MPa with the addition of gluteraldehyde [123], which is below native AF compressive properties. Aligned nanofibrous poly-ε-caprolactone scaffolds seeded with mesenchymal stem cells (MSCs) demonstrated a decreased unconfined compressive modulus of approximately 0.012 MPa, compared to 0.016 MPa of an acellular scaffold [116]. A scaffold-free AF repair strategy consisting of extracellular matrix deposited from porcine AF cells and pelleted into an implantable construct demonstrated unconfined compressive modulus of approximately 0.015 MPa, which compared well to native porcine AF tissues (0.020 MPa [124]), but was approximately an order of magnitude lower than human AF values. An AF-like scaffold with an angle ply structure made by electrospinning poly-ε-caprolactone had compressive moduli of 0.013 MPa, which was

Table 4 Summary of AF material properties

	Testing modality	Parameter		Native value	Reference
Single lamella	Uniaxial tension	E_{long}	Inner (toe/linear)	3.8/12–59 MPa	Skaggs [97], Holzapfel [98], and Stemper[a] [99]
			Outer (toe/linear)	8.01–9.67/13.2–82 MPa	Isaacs et al. [91], Skaggs [97], Holzapfel [98], Stemper[a] [99], and Wagner [108]
		E_{trans}	(Toe/linear)	0.22–1.38/1.85 MPa	Isaacs [91] and Holzapfel [98]
		$\sigma_{f,long}$		2.4–4 MPa	Isaacs [91] and Stemper[a] [99]
		$\sigma_{f,trans}$		0.33 MPa	Isaacs [91]
		$\varepsilon_{f,long}$		0.19–0.30	Isaacs [90] and Stemper[a] [99]
		$\varepsilon_{f,trans}$		0.23	Isaacs [91]
	Biaxial tension	E_z	Equibiaxial	9.88 MPa	Nagel [48]
Multiple lamellae	Uniaxial tension	E_θ	Inner (toe/linear)	1.7/2–5.6 MPa	Ebara[a] [90], Elliott [93], Shan [94], and Acaroglu[a] [100]
			Outer (toe/linear)	2.52–4.71/ 11.04–29.3 MPa	Ebara[a] [90], Isaacs et al. [91], O'Connell et al. [92], Elliott [93], Shan [94], Acaroglu[a] [100], Guerin [106], and Green [109]
		E_r	Inner	0.44 MPa	Fujita [110]
			Outer (toe/linear)	0.113–0.19/ 0.212–0.45 MPa	Isaacs [91], O'Connell [92], Elliott [93], and Fujita [110]
		E_z	Inner (toe/linear)	0.34/0.96 MPa	Elliott [93]
			Outer (toe/linear)	0.27/0.42–0.82 MPa	O'Connell [92] and Elliott [93]
		ε_θ*		0.06–0.09	O'Connell [92] and Guerin [106]
		ε_r*		0.11	O'Connell [92]
		$\nu_{\theta,z}$		1.77–2.27	O'Connell [92] and Elliott [93]
		$\nu_{\theta,r}$		0.33	Elliott [93]
		$\nu_{z,\theta}$		0.61–0.66	O'Connell [92] and Elliott [93]
		$\nu_{z,r}$		0.14	Elliott [93]
		$\nu_{r,z}$		0.51–0.79	O'Connell [92] and Elliott [93]
		$\lvert E^* \rvert$		1–3.5 MPa	Sen[a] [111]
		$\sigma_{f,\theta}$	Inner/outer	1.18/3.29–3.8 MPa	Shan [94] and Green [109]
		$\varepsilon_{f,\theta}$	Inner/outer	0.49/0.34–0.38	Shan [94] and Green [109]
	Biaxial tension	E_θ	Equibiaxial	87 MPa	O'Connell[a] [95]
		E_z	Equibiaxial	48 MPa	O'Connell[a] [95]
			Circ. Fixed	13 MPa	Bass[a] [96]
	Confined compression	P_{sw}		0.14 MPa	Best [101]
		H_A		0.40–2.5 MPa	Best [101], Iatridis [102], and Antoniou[a] [103]
		k		$2.1–5 \times 10^{-16}$ m^4/N s	Best [101], Iatridis [102], and Antoniou[a] [103]
		β		2.13	Iatridis [102]
		M		1.18	Iatridis [102]
	Shear	$\lvert G^* \rvert$		0.1–0.28 MPa	Antoniou[a] [103] and Iatridis[a] [105]
		G		0.03–0.105 MPa	Iatridis[a] [105]
		δ		9–35 deg	Iatridis[a] [105]
		G		0.02534–0.05604 MPa	Fujita [107]
	Unconfined compression	E'		0.19–0.26 MPa	Freeman[a] [104]
		E''		0.030–0.055 MPa	Freeman[a] [104]

E = Tensile modulus; E_{long} = Longitudinal modulus (parallel to fiber direction); E_{trans} = Transverse modulus (perpendicular to fiber direction); σ_f = Failure stress; ε_f = Failure strain; θ, z, r = Circumferential, axial and radial loading axes, respectively; ε^* = Transition strain; v = Poisson's ratio; $|E^*|$ = Dynamic modulus; P_{sw} = Swelling pressure; H_A = Aggregate modulus; k = Permeability; β = Modulus nonlinearity parameter; M = Permeability nonlinearity parameter; $|G^*|$ = Complex shear modulus; G = Shear modulus; δ = Phase angle; E' = Storage modulus; and E'' = Loss modulus.
[a]value estimated from figure.

significantly less than that of a native rat caudal IVD measured to be 0.28 MPa [125].

Shear modulus describes relative deformation behaviors between AF layers and is important to evaluate since failure of materials commonly occurs due to excess shear stresses. AF shear properties are nonlinear and affected by the magnitude of compressive stress on the AF [105]. An aligned nanofibrous poly-ε-caprolactone scaffold was developed and seeded with MSCs and it was observed that with time, the shear modulus increased indicating some role of cell deposited matrix components on the ability to resist shear [126]. Fibrin-Genipin exhibited shear moduli values of 0.012–0.08 MPa and could be tuned to be similar to native human AF tissue (Table 4) [127,128]. The shear modulus of an injectable, cell supportive composite hydrogel composed of hyaluronic acid and poly(ethylene glycol) demonstrated a shear moduli of 490 ± 117 Pa [129] which remains several orders of magnitude lower than native human AF tissue. At this point, no materials exist that completely match all AF material behaviors, and the most important material behavior to match is subject to debate. However, most biomaterials are not evaluated in multiple testing modes, and more thorough biomechanical assessments of biomaterials are likely to better inform material selection and performance outcomes.

Integration of biomaterials with native AF tissue remains a challenge, and current strategies use adhesives to promote integration. Adhesive strength tests measure the force required to displace a material from adjacent tissue and can be characterized with lap shear testing [26], or "pushout" testing [128]. Nerurkar et al. reported adhesive strength ~0.05–0.125 MPa from bilayer lap testing over a period of 6 weeks for a multilayered aligned nanofibrous poly-ε-caprolactone scaffold (Nerurkar et al.), suggesting good adhesion of each layer of this biomaterial. The enhanced integration of biomaterial layers with time is suggestive of long-term integration with native tissues, yet does not address acute adhesion required for postoperative success. Vernengo et al. studied adhesive strength as measured by the maximum force of detachment from porcine skin of poly(*N*-isopropylacrylamide–poly(ethylene glycol)/poly(ethylene imine) (PNIPAAm-PEG/PEI) with varied concentrations of gluteraldehyde crosslinkers and found the greatest adhesive strength was 0.0025 MPa with 10% gluteraldehyde [123], suggesting it will not resist loading on the IVD. Push-out testing of an injectable fibrin-Genipin hydrogel

Table 5 Summary of available hydrogels with tensile modulus, shear modulus, compressive modulus, adhesion strength, and gelation time.

Mechanical property	Material	Mechanical property values	References
Tensile modulus	Aligned nanofibrous poly-ε-caprolactone scaffold	5.8 ± 3.1 MPa	Nerurkar et al. [114]
	Poly(1,8-octanediol malate)	7.31–25.6 MPa[a]	Wan et al. [131]
	Aligned nanofibrous poly-ε-caprolactone scaffold	10.6–14.2 MPa[a]	Nerurkar et al. [115]
	Aligned electrospun polycarbonate polyurethane scaffold	46 ± 3 MPa	Yeganegi et al. [119]
	Electrospun PCL scaffold	2.5–7.25 MPa[a]	Koepsell et al. [118]
	Aligned nanofibrous poly-ε-caprolactone scaffold	20–35 MPa[a]	Nerurkar et al. [116]
	Aligned nanofibrous poly-ε-caprolactone scaffold ± MSCs	0.021 MPa (acellular), 0.032 MPa (cellular)[b]	Nerurkar et al. [117]
	Biodegradablepoly (d,l-lactide-co-trimethylene carbonate) networks	1.7–2.5 MPa (40 °C), 1000–1700 MPa (0 °C)	Sharifi et al. [122]
	Oriented electrospun poly(ester-urethane) and poly-ε-caprolactone	47–55.33 MPa[a]	Wismer et al. [120]
	Degradable polycarbonate urethane-anionic dihydroxyl oligomer scaffolds	3-5 MPa[a,b]	Turner et al. [121]
	Poly(*N*-isopropylacrylamide) + chondroitin sulfate + aldehyde modified chondroitin sulphate	0.001108–0.00416 MPa[a]	Wiltsey et al. [132]
Compressive modulus	Poly(*N*-isopropylacrylamide - poly(ethylene glycol)/poly(ethylene imine) aka PNIPAAm-PEG/PEI with gluteraldehyde crosslinker	0.06–0.08 MPa[a,b]	Vernengo [123]
	Aligned nanofibrous poly-ε-caprolactone scaffold ± MSCs	0.016 MPa (acellular), 0.012 MPa (cellular)[b]	Nerurkar et al. [117]
	Scaffold free neo annular tissue construct from 3D pellet culture system using mature porcine AF cells	0.015 MPa[b]	Cho et al. [124]
	Disk-like angle ply structures made by electrospinning poly-ε-caprolactone	0.0126 ± 0.0043 MPa	Martin et al. [125]
Shear Modulus	Aligned nanofibrous poly-ε-caprolactone scaffold	2.1–3.8 MPa[a,b]	Driscoll et al. [126]
	Fibrin-Genipin	0.08–0.111 MPa[a,b]	Schek et al. [127]
	Fibrin-Genipin	0.0118–0.047 MPa[a]	Guterl et al. [128]
	Hyaluronin acid-poly(ethylene glycol)	0.000109–0.00049 MPa[a]	Jeong et al. [129]
Adhesive strength	Aligned nanofibrous poly-ε-caprolactone scaffold	0.055–0.125 MPa[b]	Nerurkar et al. [115]
	Poly(*N*-isopropylacrylamide–poly(ethylene glycol)/poly(ethylene imine) with gluteraldehyde crosslinker	0.0014–0.0025 MPa[a]	Vernengo [123]
	Fibrin-Genipin	0.062–0.0722 MPa	Guterl et al. [128]
	Poly(*N*-isopropylacrylamide) + chondroitin sulfate ± aldehyde modified chondroitin sulfate	0.0011–0.0018 MPa[b]	Wiltsey et al. [132]
Gelation Time	Fibrin-Genipin	202–906 s[a]	Guterl et al. [128]
	Poly(*N*-isopropylacrylamide) + chondroitin sulfate + aldehyde modified chondroitin sulfate	600 s	Wiltsey et al. [132]

[a]The values that range for different material compositions tested within a study.
[b]Value estimated from plot.

demonstrated that adhesive strength was 0.062–0.0722, and was independent of genipin concentration [128]. PNIPAAm-*g*-CS had a relatively low adhesive strength compared to these materials, as measured by the ASTM procedure F2258 for tissue adhesives in tension, with an adhesive strength of approximately 0.001 MPa [132]. The capacity of a material to adhere strongly to native tissues immediately is an important step for clinical translation and suggests that adhesion testing is an overlooked parameter that should be performed more often to evaluating the feasibility of AF repair biomaterials to withstand physiologic loading.

Gelation time of hydrogels is an important parameter to define feasibility of clinical translation. Discectomy procedures are relatively short, and the material must stay in place following implantation. Many spine surgeries are outpatient procedures, requiring the material to withstand loads that occur following implantation as the patient recovers and returns home. In this review, only two studies reported gelation time of biomaterials for AF repair; gelation kinetics can be quantified with multiple parameters. Fibrin-Genipin had gelation time $\leq$ 15 min, as defined by the time at which the shear modulus is independent of frequency [128]. The convergence of frequency-dependent behaviors occurs following the solid/fluid transition and corresponds to sufficient solidification to stay in place [133]. PNIPAAm-*g*-CS was described to have a gelation time of 10 min for polymer gelation at 37 °C [132]. The equilibration of shear modulus to a steady state value must be achieved before the spine can bear load. These gelation times are consistent with needs for clinical translation, yet accelerated gelation kinetics are preferable.

6 Testing Paradigm

A consistent set of evaluation criteria for AF repair hydrogels can help researchers to compare across labs and more rapidly advance the field. We propose a testing paradigm that spans from rapid screening tests for optimization, in situ validation tests, and advanced validation tests (Fig. 3). Screening tests for optimization are designed to evaluate priority parameters to rapidly assess if the hydrogel will meet required design parameters. The screening tests are intended to be adaptable for high throughput testing and include the following. Material property tests to determine tensile, compressive and/or shear modulus to assess similarities with AF tissue. Adhesion strength tests to determine how strongly the hydrogel adheres to AF tissue, e.g., using a push-out or lap shear test. Cytocompatibility tests include cell culture screening to rapidly evaluate cell viability, proliferation, and phenotype of the biomaterial. Gelation kinetics (e.g., rheometer measuring shear modulus through time) evaluate if the material will solidify rapidly enough to be consistent with current surgical procedures.

Adhesive strength of a hydrogel on disk tissue can be measured directly with a lap shear test or a pushout test [128,134,135], or indirectly in situ with an increasing axial load until herniation is reached. However, test protocols, such as the adhesion strength test configuration, commonly involve tissue samples with more free-boundaries than would be found in situ which creates high shear stresses [136]. As a result, the adhesion strength parameters obtained from a screening test may be best used as a relative comparison rather than an absolute measurement value and in situ tests provide validation and failure testing that is more similar to the in vivo condition.

In situ validation tests are more involved experimentally and involve full motion segment testing and in vivo small animal tests. In vivo degradation tests involve subcutaneous and/or in situ implantation of the hydrogel in a small animal model to assess In Vivo degradation rate and inflammatory response. In situ failure tests load IVDs mechanically until failure to determine if the material has high herniation risk in situ [137]. In situ biomechanics

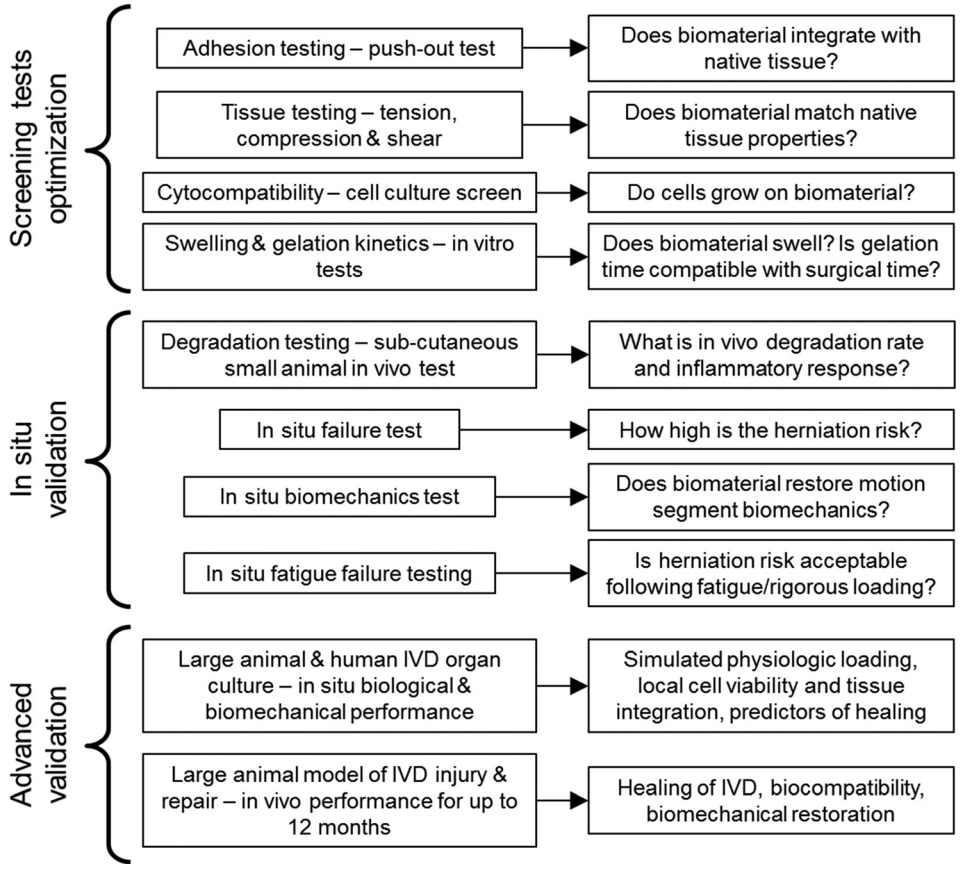

Fig. 3 Testing paradigm for evaluating IVD repair strategies. Screening tests involve high through-put evaluations that can rapidly assess materials. Testing process progresses to in vivo validation.

tests evaluate restoration of IVD mechanical properties following creation of a defect [138]. In situ failure tests can also include more rigorous fatigue loading to evaluate implant failure. Wilke et al. developed elegant testing procedures to assess AF repair implant failure under extreme and fatigue loading conditions [20]. Advanced validation tests involve testing using living animal systems. Large animal organ culture is now a common technique and can also be evaluated using human IVDs [139–142]. Human organ culture is used to assess biological and biomechanical performance such as gene expression, protein levels, tissue integration, and disk height loss. An in vivo model is necessary to assess inflammatory responses. Because of the high forces and long transport distances of human IVDs, large animal models best translate for advanced validation tests and measurements can include assessments of in vivo healing, biocompatibility, and biomechanical restoration.

The hydrogels reviewed in this paper are at various stages of development and several elegant hydrogels for AF repair exist, spanning structural multiple-layered composites as well as adhesive biomaterials with a relatively simple isotropic structure. Many experimental biomaterials for AF repair focus on their uses as carriers for drugs or cells and spend little attention on biomechanical characterizations. Characterizing mechanical properties of experimental AF repair biomaterials can better determine if the material is optimized to match AF material behaviors and functionally restore mechanics and motions of spinal motion segments. Here, we have summarized the biomechanical properties of current experimental hydrogels.

7 Quantitative Design Criteria

The adhesive strength, strain at failure, and material properties of the AF are design criteria that should be achieved, or approached for a hydrogel to successfully repair AF defects without creating stress concentrations. The data compiled in this manuscript can inform quantitative values for these parameters.

The adhesive strength of an AF repair hydrogel must resist stresses generated from intradiscal pressures during loading of the IVD. The minimum intradiscal pressures which an AF repair should withstand are 0.41 MPa (as measured in nondegenerated disks during surgery while the patient is lying prone), up to 1.50 MPa (as the patient recovers and begins sitting and standing). To prevent reherniation, the repair must withstand the greater values of intradiscal pressure expected during rigorous activity following recovery, such as 2.30 MPa, measured by Wilke et al. while lifting 20 kg with rounded back [30]. The intradiscal pressure does not directly translate to adhesive strength, especially since many biomechanical tests used to screen and characterize adhesive strength (e.g., "pushout-test," lap shear test) have different boundary conditions than the in situ condition. However, an approximation can be established using in situ biomechanical data and adhesive testing data from the literature. For example, genipin crosslinked fibrin (FibGen) had an adhesive strength of 67 kPa [128] and withstood an average nominal axial stress (force/cross-sectional area) of about 600 kPa [138]. Nachemson and Morris have proposed that nominal axial stress relates to nucleus pressure by a factor of 1.5 [34]. Therefore, an adhesive strength of 67 kPa tested using a pushout test may be able to withstand a nucleus pressure of 900 kPa. This suggests a factor of about 13.5 between pushout adhesive strength and nucleus pressure. Therefore, in order to withstand a maximum intradiscal pressure of 2.3 MPa, a hydrogel would need to achieve an adhesive strength of ~177 kPa measured with a push-out test. This adhesive strength contextualizes the experimental pushout test with in vivo loading, but is only a rough approximation since it spans multiple labs, test configurations, and experimental assumptions. Although pressures decrease in degenerated disks, an appropriate design criterion should be set at nondegenerate levels in order to provide a factor of safety.

In this review, we reviewed the in vivo ROM of the human IVD to help address the problem of failure strain and found the maximal rotation values of 13 deg, 5 deg, and 11 deg in flexion, extension, and lateral bending [44,45,51,52]. The maximal strains computed from these rotations (θ), assuming a uniform radius (r) of 27.95 mm [143] and neutral disk height (d) of 4 mm [45] and true strain (ε) $= \ln((d + r^* \tan(\theta))/d)$, are 96%, 47%, 85%, and 31%, respectively. These calculations represent a high estimate of nominal strain since the largest physiological rotations were used with the smallest disk height and largest radius. Nagel et al. and Wang et al. reported maximal tensile strains in the posterior AF of 65% and 26%, respectively, from full flexion [47,144]. The maximal compressive strain that must be withstood is 29% [48]. Therefore, the degree-of-freedom with greatest strain is flexion, putting the posterior annulus in tension, and the hydrogel must be able to withstand at least 65% strain (Table 6).

An ideal repair strategy would restore the stiffness of the intact IVD motion segment, and the torsional and axial stiffnesses values of 3.2 N m/deg and 1.5–2 kN/mm (Table 6) can be used as simplified tests to assessing AF integrity and restoration of NP pressurization [12]. The AF is loaded in tension to hold the pressurized nucleus, so it is important to match the tensile properties of the AF. Alternatively, torsion mechanics are sensitive to AF defects [13,145], so it is important to match the shear properties. The recommended tensile modulus of an AF repair varies from 0.42 to 0.82 MPa in axial testing, to 11–29 MPa in circumferential testing [90,92,93,100]; both configurations are relevant. The recommended shear modulus is 0.1–0.28 MPa [103,105] and the recommended aggregate modulus is 0.4–7 MPa [101–104] (Table 6). Stiffness values for the IVD motion segment are presented in Table 3 and complete material properties for AF tissue in Table 4. We focus on IVD stiffness for assessments of biomechanical restoration in this study, but note that in situ ROM, neutral zone, disk height, and flexibility measurements are other relevant parameters that can also be used to assess biomechanical restoration.

In conclusion, this paper summarized the biomechanical behaviors of IVD motion segments and AF tissue and used this data to provide quantitative design criteria for AF repair, specifically a test paradigm, the strain at failure, the adhesive strength, the amount of material necessary, and the tensile and shear moduli. Hydrogels for AF repair that meet these objectives can be advanced to in situ and advanced validation tests to better assess their likelihood for successful performance in humans. We propose a testing paradigm from least complex screening and optimization tests to more complex in situ and in vivo validation tests in order to efficiently and effectively screen biomaterials for AF repair. In order to advance to in vivo validation tests, we suggest that successful materials have high adhesion strength (~0.2 MPa), have high tensile failure strain (~65%), and match as many AF material properties as possible (e.g., approximately 1 MPa, 0.3 MPa, and 30 MPa for compressive, shear, and tensile moduli, respectively). Several tissue engineered hydrogels exist and show promise for AF repair since they can match at least one material property of the AF, and a few of these hydrogels can also adhere to AF tissue or otherwise be easily implanted during surgical procedures to warrant additional investigation.

Table 6 Recommended design parameters

Parameter	Recommended value	Reference
Disk pressure, after implantation	1.50 MPa	Fig. 1
Disk pressure, maximal	2.30 MPa	[30]
Tensile modulus, axial	0.5–1 MPa	Fig. 2, Table 4
Compressive/tensile strain	28%/65%	Table 2
Axial stiffness of restored IVD	1.5–2 kN/mm	Table 3
Torsional stiffness of restored IVD	3.2 N m/deg	Table 3
Tensile modulus, circumferential	11–29 MPa	Fig. 2, Table 4
Aggregate modulus	0.4–6 MPa	Table 4
Shear modulus	0.1–0.28 MPa	Table 4

Acknowledgment

The authors thank Dr. Hironobu Watanabe of Keiyu Orthopedic Hospital for translating the Japanese text of Okushima et al. 1970 into English. Supported by grants from: the National Institute of Arthritis and Musculoskeletal and Skin Diseases of the National Institutes of Health R01AR057397; Collaborative Research Partner Program on Annulus Fibrosus Rupture of the AO Foundation, Davos, Switzerland; and Traineeship, the National Institute of General Medical Science of the NIH Integrated Pharmacological Sciences Training Program T32 GM062754.

Nomenclature

AF = annulus fibrosus
IVD = intervertebral disk
MSC = mesenchymal stem cell
NP = nucleus pulposus
ROM = range of motion

References

[1] Vos, T., Flaxman, A. D., Naghavi, M., Lozano, R., Michaud, C., Ezzati, M., Shibuya, K., Salomon, J. A., Abdalla, S., Aboyans, V., Abraham, J., Ackerman, I., Aggarwal, R., Ahn, S. Y., Ali, M. K., AlMazroa, M. A., Alvarado, M., Anderson, H. R., Anderson, L. M., Andrews, K. G., Atkinson, C., Baddour, L. M., Bahalim, A. N., Barker-Collo, S., Barrero, L. H., Bartels, D. H., Basáñez, M.-G., Baxter, A., Bell, M. L., Benjamin, E. J., Bennett, D., Bernabé, E., Bhalla, K., Bhandari, B., Bikbov, B., Abdulhak, A. B., Birbeck, G., Black, J. A., Blencowe, H., Blore, J. D., Blyth, F., Bolliger, I., Bonaventure, A., Boufous, S., Bourne, R., Boussinesq, M., Braithwaite, T., Brayne, C., Bridgett, L., Brooker, S., Brooks, P., Brugha, T. S., Bryan-Hancock, C., Bucello, C., Buchbinder, R., Buckle, G., Budke, C. M., Burch, M., Burney, P., Burstein, R., Calabria, B., Campbell, B., Canter, C. E., Carabin, H., Carapetis, J., Carmona, L., Cella, C., Charlson, F., Chen, H., Cheng, A. T.-A., Chou, D., Chugh, S. S., Coffeng, L. E., Colan, S. D., Colquhoun, S., Colson, K. E., Condon, J., Connor, M. D., Cooper, L. T., Corriere, M., Cortinovis, M., Courville de Vaccaro, K., Couser, W., Cowie, B. C., Criqui, M. H., Cross, M., Dabhadkar, K. C., Dahiya, M., Dahodwala, N., Damsere-Derry, J., Danaei, G., Davis, A., De Leo, D., Degenhardt, L., Dellavalle, R., Delossantos, A., Denenberg, J., Derrett, S., Des Jarlais, D. C., Dharmaratne, S. D., Dherani, M., Diaz-Torne, C., Dolk, H., Dorsey, E. R., Driscoll, T., Duber, H., Ebel, B., Edmond, K., Elbaz, A., Eltahir Ali, S., Erskine, H., Erwin, P. J., Espindola, P., Ewoigbokhan, S. E., Farzadfar, F., Feigin, V., Felson, D. T., Ferrari, A., Ferri, C. P., Fèvre, E. M., Finucane, M. M., Flaxman, S., Flood, L., Foreman, K., Forouzanfar, M. H., Fowkes, F. G. R., Franklin, R., Fransen, M., Freeman, M. K., Gabbe, B. J., Gabriel, S. E., Gakidou, E., Ganatra, H. A., Garcia, B., Gaspari, F., Gillum, R. F., Gmel, G., Gosselin, R., Grainger, R., Groeger, J., Guillemin, F., Gunnell, D., Gupta, R., Haagsma, J., Hagan, H., Halasa, Y. A., Hall, W., Haring, D., Haro, J. M., Harrison, J. E., Havmoeller, R., Hay, R. J., Higashi, H., Hill, C., Hoen, B., Hoffman, H., Hotez, P. J., Hoy, D., Huang, J. J., Ibeanusi, S. E., Jacobsen, K. H., James, S. L., Jarvis, D., Jasrasaria, R., Jayaraman, S., Johns, N., Jonas, J. B., Karthikeyan, G., Kassebaum, N., Kawakami, N., Keren, A., Khoo, J.-P., King, C. H., Knowlton, L. M., Kobusingye, O., Koranteng, A., Krishnamurthi, R., Lalloo, R., Laslett, L. L., Lathlean, T., Leasher, J. L., Lee, Y. Y., Leigh, J., Lim, S. S., Limb, E., Lin, J. K., Lipnick, M., Lipshultz, S. E., Liu, W., Loane, M., Lockett Ohno, S., Lyons, R., Ma, J., Mabweijano, J., MacIntyre, M. F., Malekzadeh, R., Mallinger, L., Manivannan, S., Marcenes, W., March, L., Margolis, D. J., Marks, G. B., Marks, R., Matsumori, A., Matzopoulos, R., Mayosi, B. M., McAnulty, J. H., McDermott, M. M., McGill, N., McGrath, J., Medina-Mora, M. E., Meltzer, M., Memish, Z. A., Mensah, G. A., Merriman, T. R., Meyer, A.-C., Miglioli, V., Miller, M., Miller, T. R., Mitchell, P. B., Mocumbi, A. O., Moffitt, T. E., Mokdad, A. A., Monasta, L., Montico, M., Moradi-Lakeh, M., Moran, A., Morawska, L., Mori, R., Murdoch, M. E., Mwaniki, M. K., Naidoo, K., Nair, M. N., Naldi, L., Narayan, K. M. V., Nelson, P. K., Nelson, R. G., Nevitt, M. C., Newton, C. R., Nolte, S., Norman, P., Norman, R., O'Donnell, M., O'Hanlon, S., Olives, C., Omer, S. B., Ortblad, K., Osborne, R., Ozgediz, D., Page, A., Pahari, B., Pandian, J. D., Panozo Rivero, A., Patten, S. B., Pearce, N., Perez Padilla, R., Perez-Ruiz, F., Perico, N., Pesudovs, K., Phillips, D., Phillips, M. R., Pierce, K., Pion, S., Polanczyk, G. V., Polinder, S., Pope III, C. A., Popova, S., Porrini, E., Pourmalek, F., Prince, M., Pullan, R. L., Ramaiah, K. D., Ranganathan, D., Razavi, H., Regan, M., Rehm, J. T., Rein, D. B., Remuzzi, G., Richardson, K., Rivara, F. P., Roberts, T., Robinson, C., Rodriguez De Leòn, F., Ronfani, L., Room, R., Rosenfeld, L. C., Rushton, L., Sacco, R. L., Saha, S., Sampson, U., Sanchez-Riera, L., Sanman, E., Schwebel, D. C., Scott, J. G., Segui-Gomez, M., Shahraz, S., Shepard, D. S., Shin, H., Shivakoti, R., Silberberg, D., Singh, D., Singh, G. M., Singh, J. A., Singleton, J., Sleet, D. A., Sliwa, K., Smith, E., Smith, J. L., Stapelberg, N. J. C., Steer, A., Steiner, T., Stolk, W. A., Stovner, L. J., Sudfeld, C., Syed, S., Tamburlini, G., Tavakkoli, M., Taylor, H. R., Taylor, J. A., Taylor, W. J., Thomas, B., Thomson, W. M., Thurston, G. D., Tleyjeh, I. M., Tonelli, M., Towbin, J. A., Truelsen, T., Tsilimbaris, M. K., Ubeda, C., Undurraga, E. A., van der Werf, M. J., van Os, J., Vavilala, M. S., Venketasubramanian, N., Wang, M., Wang, W., Watt, K., Weatherall, D. J., Weinstock, M. A., Weintraub, R., Weisskopf, M. G., Weissman, M. M., White, R. A., Whiteford, H., Wiersma, S. T., Wilkinson, J. D., Williams, H. C., Williams, S. R. M., Witt, E., Wolfe, F., Woolf, A. D., Wulf, S., Yeh, P.-H., Zaidi, A. K. M., Zheng, Z.-J., Zonies, D., Lopez, A. D., and Murray, C. J. L., 2012, "Years Lived With Disability (YLDs) for 1160 Sequelae of 289 Diseases and Injuries 1990–2010: A Systematic Analysis for the Global Burden of Disease Study 2010," Lancet, **380**(9859), pp. 2163–2196.

[2] March, L., Smith, E. U. R., Hoy, D. G., Cross, M. J., Sanchez-Riera, L., Blyth, F., Buchbinder, R., Vos, T., and Woolf, A. D., 2014, "Burden of Disability Due to Musculoskeletal (MSK) Disorders," Best Pract. Res. Clin. Rheumatol., **28**(3), pp. 353–366.

[3] Weinstein, J. N., Lurie, J. D., Tosteson, T. D., Skinner, J. S., Hanscom, B., Tosteson, A. N. A., Herkowitz, H., Fischgrund, J., Cammisa, F. P., Albert, T., and Deyo, R. A., 2006, "Surgical versus Nonoperative Treatment for Lumbar Disk Herniation: The Spine Patient Outcomes Research Trial (SPORT) Observational Cohort," JAMA, **296**(20), pp. 2451–2459.

[4] Weinstein, J. N., Lurie, J. D., Tosteson, T. D., Tosteson, A. N. A., Blood, E. A., Abdu, W. A., Herkowitz, H., Hilibrand, A., Albert, T., and Fischgrund, J., 2008, "Surgical Versus Nonoperative Treatment for Lumbar Disc Herniation: Four-Year Results for the Spine Patient Outcomes Research Trial (SPORT)," Spine, **33**(25), pp. 2789–2800.

[5] Asch, H. L., Lewis, P. J., Moreland, D. B., Egnatchik, J. G., Yu, Y. J., Clabeaux, D. E., and Hyland, A. H., 2002, "Prospective Multiple Outcomes Study of Outpatient Lumbar Microdiscectomy: Should 75 to 80% Success Rates be the Norm?," J. Neurosurg., **96**(1 Suppl.), pp. 34–44.

[6] Gray, D. T., Deyo, R. A., Kreuter, W., Mirza, S. K., Heagerty, P. J., Comstock, B. A., and Chan, L., 2006, "Population-Based Trends in Volumes and Rates of Ambulatory Lumbar Spine Surgery," Spine, **31**(17), pp. 1957–1964.

[7] McGirt, M. J., Eustacchio, S., Varga, P., Vilendecic, M., Trummer, M., Gorensek, M., Ledic, D., and Carragee, E. J., 2009, "A Prospective Cohort Study of Close Interval Computed Tomography and Magnetic Resonance Imaging After Primary Lumbar Discectomy: Factors Associated With Recurrent Disc Herniation and Disc Height Loss," Spine, **34**(19), pp. 2044–2051.

[8] Watters, W. C., and McGirt, M. J., 2009, "An Evidence-Based Review of the Literature on the Consequences of Conservative Versus Aggressive Discectomy for the Treatment of Primary Disc Herniation With Radiculopathy," Spine J., **9**(3), pp. 240–257.

[9] Ambrossi, G. L. G., McGirt, M. J., Sciubba, D. M., Witham, T. F., Wolinsky, J.-P., Gokaslan, Z. L., and Long, D. M., 2009, "Recurrent Lumbar Disc Herniation After Single-Level Lumbar Discectomy," Neurosurgery, **65**(3), pp. 574–578.

[10] Iatridis, J. C., MacLean, J. J., Roughley, P. J., and Alini, M., 2006, "Effects of Mechanical Loading on Intervertebral Disc Metabolism In Vivo," J. Bone Joint Surg. Am., **88**(Suppl. 2), pp. 41–46.

[11] Elliott, D. M., Yerramalli, C. S., Beckstein, J. C., Boxberger, J. I., Johannessen, W., and Vresilovic, E. J., 2008, "The Effect of Relative Needle Diameter in Puncture and Sham Injection Animal Models of Degeneration," Spine, **33**(6), pp. 588–596.

[12] Iatridis, J. C., Nicoll, S. B., Michalek, A. J., Walter, B. A., and Gupta, M. S., 2013, "Role of Biomechanics in Intervertebral Disc Degeneration and Regenerative Therapies: What Needs Repairing in the Disc and What are Promising Biomaterials for its Repair?," Spine J., **13**(3), pp. 243–262.

[13] Michalek, A. J., and Iatridis, J. C., 2012, "Height and Torsional Stiffness are Most Sensitive to Annular Injury in Large Animal Intervertebral Discs," Spine J., **12**(5), pp. 425–432.

[14] Masuda, K., Aota, Y., Muehleman, C., Imai, Y., Okuma, M., Thonar, E. J., Andersson, G. B., and An, H. S., 2005, "A Novel Rabbit Model of Mild, Reproducible Disc Degeneration by an Anulus Needle Puncture: Correlation Between the Degree of Disc Injury and Radiological and Histological Appearances of Disc Degeneration," Spine, **30**(1), pp. 5–14.

[15] Melrose, J., Roberts, S., Smith, S., Menage, J., and Ghosh, P., 2002, "Increased Nerve and Blood Vessel Ingrowth Associated With Proteoglycan Depletion in an Ovine Anular Lesion Model of Experimental Disc Degeneration," Spine, **27**(12), pp. 1278–1285.

[16] Freemont, A. J., Peacock, T. E., Goupille, P., Hoyland, J. A., O'Brien, J., and Jayson, M. I., 1997, "Nerve Ingrowth Into Diseased Intervertebral Disc in Chronic Back Pain," Lancet, **350**(9072), pp. 178–181.

[17] Ahlgren, B. D., Lui, W., Herkowitz, H. N., Panjabi, M. M., and Guiboux, J. P., 2000, "Effect of Anular Repair on the Healing Strength of the Intervertebral Disc: A Sheep Model," Spine, **25**(17), pp. 2165–2170.

[18] Bailey, A., Araghi, A., Blumenthal, S., and Huffmon, G. V., 2013, "Prospective, Multicenter, Randomized, Controlled Study of Anular Repair in Lumbar Discectomy," Spine, **38**(14), pp. 1161–1169.

[19] Lequin, M. B., Barth, M., Thomé, C., and Bouma, G. J., 2012, "Primary Limited Lumbar Discectomy With an Annulus Closure Device: One-Year Clinical and Radiographic Results From a Prospective, Multi-Center Study," Korean J. Spine, **9**(4), pp. 340–347.

[20] Wilke, H.-J., Ressel, L., Heuer, F., Graf, N., and Rath, S., 2013, "Can Prevention of a Reherniation be Investigated? Establishment of a Herniation Model and Experiments With an Anular Closure Device," Spine, **38**(10), pp. E587–E593.

[21] Trummer, M., Eustacchio, S., Barth, M., Klassen, P. D., and Stein, S., 2013, "Protecting Facet Joints Post-Lumbar Discectomy: Barricaid Annular Closure Device Reduces Risk of Facet Degeneration," Clin. Neurol. Neurosurg., **115**(8), pp. 1440–1445.

[22] Masuda, K., and Lotz, J. C., 2010, "New Challenges for Intervertebral Disc Treatment Using Regenerative Medicine," Tissue Eng. Part B: Rev., **16**(1), pp. 147–158.

[23] Sakai, D., and Andersson, G. B. J., 2015, "Stem Cell Therapy for Intervertebral Disc Regeneration: Obstacles and Solutions," Nat. Rev. Rheumatol., **11**(4), pp. 243–256.
[24] Guterl, C. C., See, E. Y., Blanquer, S. B. G., Pandit, A., Ferguson, S. J., Benneker, L. M., Grijpma, D. W., Sakai, D., Eglin, D., Alini, M., Iatridis, J. C., and Grad, S., 2013, "Challenges and Strategies in the Repair of Ruptured Annulus Fibrosus," Eur. Cell Mater., **25**, pp. 1–21.
[25] Kandel, R., Roberts, S., and Urban, J. P. G., 2008, "Tissue Engineering and the Intervertebral Disc: The Challenges," Eur. Spine J., **17**(S4), pp. 480–491.
[26] Nerurkar, N. L., Elliott, D. M., and Mauck, R. L., 2010, "Mechanical Design Criteria for Intervertebral Disc Tissue Engineering," J. Biomech., **43**(6), pp. 1017–1030.
[27] Likhitpanichkul, M., Dreischarf, M., Illien-Junger, S., Walter, B. A., Nukaga, T., Long, R. G., Sakai, D., Hecht, A. C., and Iatridis, J. C., 2014, "Fibrin-Genipin Adhesive Hydrogel for Annulus Fibrosus Repair: Performance Evaluation With Large Animal Organ Culture, In Situ Biomechanics, and In Vivo Degradation Tests," Eur. Cell Mater., **28**, pp. 25–38.
[28] Quinnell, R. C., Stockdale, H. R., and Willis, D. S., 1983, "Observations of Pressures Within Normal Discs in the Lumbar Spine," Spine, **8**(2), pp. 166–169.
[29] Nachemson, A., and Elfstrom, G., 1970, "Intravital Dynamic Pressure Measurements in Lumbar Discs. A Study of Common Movements, Maneuvers and Exercises," Scand. J. Rehabil. Med. Suppl., **1**, pp. 1–40.
[30] Wilke, H. J., Neef, P., Caimi, M., Hoogland, T., and Claes, L. E., 1999, "New In Vivo Measurements of Pressures in the Intervertebral Disc in Daily Life," Spine, **24**(8), pp. 755–762.
[31] Sato, K., Kikuchi, S., and Yonezawa, T., 1999, "In Vivo Intradiscal Pressure Measurement in Healthy Individuals and in Patients With Ongoing Back Problems," Spine, **24**(23), pp. 2468–2474.
[32] Schultz, A., Andersson, G., Ortengren, R., Haderspeck, K., and Nachemson, A., 1982, "Loads on the Lumbar Spine. Validation of a Biomechanical Analysis by Measurements of Intradiscal Pressures and Myoelectric Signals," J. Bone Joint Surg. Am., **64**(5), pp. 713–720.
[33] Okushima, H., 1970, "Study on Hydrodynamic Pressure of Lumbar Intervertebral Disc," Nihon Geka Hokan, **39**(1), pp. 45–57.
[34] Nachemson, A., and Morris, J. M., 1964, "In Vivo Measurements of Intradiscal Pressure. Discometry, A Method for the Determination of the Pressure in the Lower Lumbar Discs," J. Bone Joint Surg. Am., **46**, pp. 1077–1092.
[35] Nachemson, A., 1965, "The Effect of Forward Leaning on Lumbar Intradiscal Pressure," Acta Orthop. Scand., **35**, pp. 314–328.
[36] Nachemson, A., 1966, "The Load on Lumbar Disks in Different Positions of the Body," Clin. Orthop. Relat. Res., **45**, pp. 107–122.
[37] Andersson, B. J., and Ortengren, R., 1974, "Lumbar Disc Pressure and Myoelectric Back Muscle Activity During Sitting. 3. Studies on a Wheelchair," Scand. J. Rehabil. Med., **6**(3), pp. 122–127.
[38] Andersson, B. J., and Ortengren, R., 1974, "Lumbar Disc Pressure and Myoelectric Back Muscle Activity During Sitting. II. Studies on an Office Chair," Scand. J. Rehabil. Med., **6**(3), pp. 115–121.
[39] Andersson, G. B., Ortengren, R., and Nachemson, A., 1977, "Intradiskal Pressure, Intra-Abdominal Pressure and Myoelectric Back Muscle Activity Related to Posture and Loading," Clin. Orthop. Relat. Res., **129**, pp. 156–164.
[40] Adams, M. A., and Hutton, W. C., 1980, "The Effect of Posture on the Role of the Apophysial Joints in Resisting Intervertebral Compressive Forces," J. Bone Joint Surg. Br., **62**(3), pp. 358–362.
[41] Claus, A., Hides, J., Moseley, G. L., and Hodges, P., 2008, "Sitting Versus Standing: Does the Intradiscal Pressure Cause Disc Degeneration or Low Back Pain?," J. Electromyogr. Kinesiol., **18**(4), pp. 550–558.
[42] Nachemson, A., 1960, "Lumbar Intradiscal Pressure. Experimental Studies on Post-Mortem Material," Acta Orthop. Scand. Suppl., **43**, pp. 1–104.
[43] Merriam, W. F., Quinnell, R. C., Stockdale, H. R., and Willis, D. S., 1984, "The Effect of Postural Changes on the Inferred Pressures Within the Nucleus Pulposus During Lumbar Discography," Spine, **9**(4), pp. 405–408.
[44] Pearcy, M., Portek, I., and Shepherd, J., 1984, "Three-Dimensional X-Ray Analysis of Normal Movement in the Lumbar Spine," Spine, **9**(3), pp. 294–297.
[45] Pearcy, M. J., and Tibrewal, S. B., 1984, "Axial Rotation and Lateral Bending in the Normal Lumbar Spine Measured by Three-Dimensional Radiography," Spine, **9**(6), pp. 582–587.
[46] Lee, S.-H., Daffner, S. D., and Wang, J. C., 2014, "Does Lumbar Disk Degeneration Increase Segmental Mobility In Vivo? Segmental Motion Analysis of the Whole Lumbar Spine Using Kinetic MRI," J. Spinal Disord. Tech., **27**(2), pp. 111–116.
[47] Nagel, T. M., Zitnay, J. L., Barocas, V. H., and Nuckley, D. J., 2014, "Quantification of Continuous In Vivo Flexion–Extension Kinematics and Intervertebral Strains," Eur. Spine J., **23**(4), pp. 754–761.
[48] Nagel, T. M., Hadi, M. F., Claeson, A. A., Nuckley, D. J., and Barocas, V. H., 2014, "Combining Displacement Field and Grip Force Information to Determine Mechanical Properties of Planar Tissue With Complicated Geometry," ASME J. Biomech. Eng., **136**(11), p. 114501.
[49] Kanayama, M., Tadano, S., Kaneda, K., Ukai, T., Abumi, K., and Ito, M., 1995, "A Cineradiographic Study on the Lumbar Disc Deformation During Flexion and Extension of the Trunk," Clin. Biomech. (Bristol, Avon), **10**(4), pp. 193–199.
[50] Zhong, W., Driscoll, S. J., Wu, M., Wang, S., Liu, Z., Cha, T. D., Wood, K. B., and Li, G., 2014, "In Vivo Morphological Features of Human Lumbar Discs," Medicine, **93**(28), p. e333.
[51] Pearcy, M. J., and Tibrewal, S. B., 1984, "Lumbar Intervertebral Disc and Ligament Deformations Measured In Vivo," Clin. Orthop. Relat. Res., **191**, pp. 281–286.
[52] Aiyangar, A. K., Zheng, L., Tashman, S., Anderst, W. J., and Zhang, X., 2014, "Capturing Three-Dimensional In Vivo Lumbar Intervertebral Joint Kinematics Using Dynamic Stereo-X-Ray Imaging," ASME J. Biomech. Eng., **136**(1), p. 011004.
[53] Miao, J., Wang, S., Wan, Z., Park, W. M., Xia, Q., Wood, K., and Li, G., 2013, "Motion Characteristics of the Vertebral Segments With Lumbar Degenerative Spondylolisthesis in Elderly Patients," Eur. Spine J., **22**(2), pp. 425–431.
[54] Stokes, I. A., and Frymoyer, J. W., 1987, "Segmental Motion and Instability," Lumbar Intradiscal Pressure: Experimental Studies on Post-Mortem Material, **12**(7), pp. 688–691.
[55] Li, G., Wang, S., Passias, P., Xia, Q., Li, G., and Wood, K., 2009, "Segmental In Vivo Vertebral Motion During Functional Human Lumbar Spine Activities," Eur. Spine J., **18**(7), pp. 1013–1021.
[56] Xia, Q., Wang, S., Kozanek, M., Passias, P., Wood, K., and Li, G., 2010, "In-Vivo Motion Characteristics of Lumbar Vertebrae in Sagittal and Transverse Planes," J. Biomech., **43**(10), pp. 1905–1909.
[57] Wang, S., Xia, Q., Passias, P., Li, W., Wood, K., and Li, G., 2011, "How Does Lumbar Degenerative Disc Disease Affect the Disc Deformation at the Cephalic Levels In Vivo?," Spine, **36**(9), pp. E574–E581.
[58] Yoder, J. H., Peloquin, J. M., Song, G., Tustison, N. J., Moon, S. M., Wright, A. C., Vresilovic, E. J., Gee, J. C., and Elliott, D. M., 2014, "Internal Three-Dimensional Strains in Human Intervertebral Discs Under Axial Compression Quantified Noninvasively by Magnetic Resonance Imaging and Image Registration," ASME J. Biomech. Eng., **136**(11), p. 111008.
[59] Stokes, I. A., 1987, "Surface Strain on Human Intervertebral Discs," J. Orthop. Res., **5**(3), pp. 348–355.
[60] Nachemson, A. L., Schultz, A. B., and Berkson, M. H., 1979, "Mechanical Properties of Human Lumbar Spine Motion Segments. Influence of Age, Sex, Disc Level, and Degeneration," Spine, **4**(1), pp. 1–8.
[61] Shea, M., Takeuchi, T. Y., Wittenberg, R. H., White, A. A., and Hayes, W. C., 1994, "A Comparison of the Effects of Automated Percutaneous Diskectomy and Conventional Diskectomy on Intradiscal Pressure, Disk Geometry, and Stiffness," J. Spinal Disord., **7**(4), pp. 317–325.
[62] Beckstein, J. C., Sen, S., Schaer, T. P., Vresilovic, E. J., and Elliott, D. M., 2008, "Comparison of Animal Discs Used in Disc Research to Human Lumbar Disc: Axial Compression Mechanics and Glycosaminoglycan Content," Spine, **33**(6), pp. E166–E173.
[63] Gardner-Morse, M. G., and Stokes, I. A. F., 2004, "Structural Behavior of Human Lumbar Spinal Motion Segments," J. Biomech., **37**(2), pp. 205–212.
[64] Lu, W. W., Luk, K. D. K., Holmes, A. D., Cheung, K. M. C., and Leong, J. C. Y., 2005, "Pure Shear Properties of Lumbar Spinal Joints and the Effect of Tissue Sectioning on Load Sharing," Spine, **30**(8), pp. E204–E209.
[65] Showalter, B. L., Beckstein, J. C., Martin, J. T., Beattie, E. E., Espinoza Orías, A. A., Schaer, T. P., Vresilovic, E. J., and Elliott, D. M., 2012, "Comparison of Animal Discs Used in Disc Research to Human Lumbar Disc: Torsion Mechanics and Collagen Content," Spine, **37**(15), pp. E900–E907.
[66] Thompson, R. E., Pearcy, M. J., Downing, K. J., Manthey, B. A., Parkinson, I. H., and Fazzalari, N. L., 2000, "Disc Lesions and the Mechanics of the Intervertebral Joint Complex," Spine, **25**(23), pp. 3026–3035.
[67] Marini, G., Huber, G., Püschel, K., and Ferguson, S. J., 2015, "Nonlinear Dynamics of the Human Lumbar Intervertebral Disc," J. Biomech., **48**(3), pp. 479–488.
[68] O'Connell, G. D., Jacobs, N. T., Sen, S., Vresilovic, E. J., and Elliott, D. M., 2011, "Axial Creep Loading and Unloaded Recovery of the Human Intervertebral Disc and the Effect of Degeneration," J. Mech. Behav. Biomed. Mater., **4**(7), pp. 933–942.
[69] Landham, P. R., Baker-Rand, H. L. A., Gilbert, S. J., Pollintine, P., Annesley-Williams, D. J., Adams, M. A., and Dolan, P., 2015, "Is kyphoplasty Better Than Vertebroplasty at Restoring Form and Function After Severe Vertebral Wedge Fractures?," Spine J., **15**(4), pp. 721–732.
[70] Frei, H., Oxland, T. R., and Nolte, L. P., 2002, "Thoracolumbar Spine Mechanics Contrasted Under Compression and Shear Loading," J. Orthop. Res., **20**(6), pp. 1333–1338.
[71] Okawa, A., Shinomiya, K., Takakuda, K., and Nakai, O., 1996, "A Cadaveric Study on the Stability of Lumbar Segment After Partial Laminotomy and Facetectomy With Intact Posterior Ligaments," J. Spinal Disord., **9**(6), pp. 518–526.
[72] McGlashen, K. M., Miller, J. A., Schultz, A. B., and Andersson, G. B., 1987, "Load Displacement Behavior of the Human Lumbo-Sacral Joint," J. Orthop. Res., **5**(4), pp. 488–496.
[73] Kiehl, K. L., Curry, W. H., Stemper, B. D., Eckardt, G., Basiden, J. L., Maiman, D. J., Yoganandan, N., and Shender, B. S., 2014, "A Method for Inducing and Determining Biomechanics Associated With Endplate Fractures in the Lumbar Spine," Biomed. Sci. Instrum., **50**, pp. 119–124.
[74] Gardner-Morse, M. G., and Stokes, I. A., 2003, "Physiological Axial Compressive Preloads Increase Motion Segment Stiffness, Linearity and Hysteresis in all Six Degrees of Freedom for Small Displacements About the Neutral Posture," J. Orthop. Res., **21**(3), pp. 547–552.
[75] Izambert, O., Mitton, D., Thourot, M., and Lavaste, F., 2003, "Dynamic Stiffness and Damping of Human Intervertebral Disc Using Axial Oscillatory Displacement Under a Free Mass System," Eur. Spine J., **12**(6), pp. 562–566.
[76] Costi, J. J., Stokes, I. A., Gardner-Morse, M. G., and Iatridis, J. C., 2008, "Frequency-Dependent Behavior of the Intervertebral Disc in Response to Each of Six Degree of Freedom Dynamic Loading: Solid Phase and Fluid Phase Contributions," Spine, **33**(16), pp. 1731–1738.

[77] Smeathers, J. E., and Joanes, D. N., 1988, "Dynamic Compressive Properties of Human Lumbar Intervertebral Joints: A Comparison Between Fresh and Thawed Specimens," J. Biomech., **21**(5), pp. 425–433.
[78] Alkalay, R. N., Vader, D., and Hackney, D., 2015, "The Degenerative State of the Intervertebral Disk Independently Predicts the Failure of Human Lumbar Spine to High Rate Loading: An Experimental Study," Clin. Biomech. (Bristol, Avon)., **30**(2), pp. 211–218.
[79] Keller, T. S., Spengler, D. M., and Hansson, T. H., 1987, "Mechanical Behavior of the Human Lumbar Spine. I. Creep Analysis During Static Compressive Loading," J. Orthop. Res., **5**(4), pp. 467–478.
[80] Amin, D. B., Lawless, I. M., Sommerfeld, D., Stanley, R. M., Ding, B., and Costi, J. J., 2015, "Effect of Potting Technique on the Measurement of Six Degree-of-Freedom Viscoelastic Properties of Human Lumbar Spine Segments," ASME J. Biomech. Eng., **137**(5), p. 054501.
[81] Zirbel, S. A., Stolworthy, D. K., Howell, L. L., and Bowden, A. E., 2013, "Intervertebral Disc Degeneration Alters Lumbar Spine Segmental Stiffness in all Modes of Loading Under a Compressive Follower Load," Spine J., **13**(9), pp. 1134–1147.
[82] Schmidt, T. A., An, H. S., Lim, T. H., Nowicki, B. H., and Haughton, V. M., 1998, "The Stiffness of Lumbar Spinal Motion Segments With a High-Intensity Zone in the Anulus Fibrosus," Spine, **23**(20), pp. 2167–2173.
[83] Haughton, V. M., Lim, T. H., and An, H., 1999, "Intervertebral Disk Appearance Correlated With Stiffness of Lumbar Spinal Motion Segments," AJNR Am. J. Neuroradiol., **20**(6), pp. 1161–1165.
[84] Garges, K. J., Nourbakhsh, A., Morris, R., Yang, J., Mody, M., and Patterson, R., 2008, "A Comparison of the Torsional Stiffness of the Lumbar Spine in Flexion and Extension," J. Manipulat. Physiol. Ther., **31**(8), pp. 1–7.
[85] Brown, M. D., Holmes, D. C., and Heiner, A. D., 2002, "Measurement of Cadaver Lumbar Spine Motion Segment Stiffness," Spine, **27**(9), pp. 918–922.
[86] Miller, J. A., Schultz, A. B., Warwick, D. N., and Spencer, D. L., 1986, "Mechanical Properties of Lumbar Spine Motion Segments Under Large Loads," J. Biomech., **19**(1), pp. 79–84.
[87] Bisschop, A., Mullender, M. G., Kingma, I., Jiya, T. U., van der Veen, A. J., Roos, J. C., van Dieën, J. H., and van Royen, B. J., 2011, "The Impact of Bone Mineral Density and Disc Degeneration on Shear Strength and Stiffness of the Lumbar Spine Following Laminectomy," Eur. Spine J., **21**(3), pp. 530–536.
[88] Bisschop, A., van Royen, B. J., Mullender, M. G., Paul, C. P. L., Kingma, I., Jiya, T. U., van der Veen, A. J., and van Dieën, J. H., 2012, "Which Factors Prognosticate Spinal Instability Following Lumbar Laminectomy?," Eur. Spine J., **21**(12), pp. 2640–2648.
[89] Cassidy, J. J., Hiltner, A., and Baer, E., 1989, "Hierarchical Structure of the Intervertebral Disc," Connect. Tissue Res., **23**(1), pp. 75–88.
[90] Ebara, S., Iatridis, J. C., Setton, L. A., Foster, R. J., Mow, V. C., and Weidenbaum, M., 1996, "Tensile Properties of Nondegenerate Human Lumbar Anulus Fibrosus," Spine, **21**(4), pp. 452–461.
[91] Isaacs, J. L., Vresilovic, E., Sarkar, S., and Marcolongo, M., 2014, "Role of Biomolecules on Annulus Fibrosus Micromechanics_ Effect of Enzymatic Digestion on Elastic and Failure Properties," J. Mech. Behav. Biomed. Mater., **40**(C), pp. 75–84.
[92] O'Connell, G. D., Guerin, H. L., and Elliott, D. M., 2009, "Theoretical and Uniaxial Experimental Evaluation of Human Annulus Fibrosus Degeneration," ASME J. Biomech. Eng., **131**(11), p. 111007.
[93] Elliott, D. M., and Setton, L. A., 2001, "Anisotropic and Inhomogeneous Tensile Behavior of the Human Anulus Fibrosus: Experimental Measurement and Material Model Predictions," ASME J. Biomech. Eng., **123**(3), p. 256.
[94] Shan, Z., Li, S., Liu, J., Mamuti, M., Wang, C., and Zhao, F., 2015, "Correlation Between Biomechanical Properties of the Annulus Fibrosus and Magnetic Resonance Imaging (MRI) Findings," Eur. Spine J., **24**(9), pp. 1909–1916.
[95] O'Connell, G. D., Sen, S., and Elliott, D. M., 2012, "Human Annulus Fibrosus Material Properties From Biaxial Testing and Constitutive Modeling are Altered With Degeneration," Biomech. Model. Mechanobiol., **11**(3–4), pp. 493–503.
[96] Bass, E. C., Ashford, F. A., Segal, M. R., and Lotz, J. C., 2004, "Biaxial Testing of Human Annulus Fibrosus and its Implications for a Constitutive Formulation," Ann. Biomed. Eng., **32**(9), pp. 1231–1242.
[97] Skaggs, D. L., Weidenbaum, M., Iatridis, J. C., Ratcliffe, A., and Mow, V. C., 1994, "Regional Variation in Tensile Properties and Biochemical Composition of the Human Lumbar Anulus Fibrosus," Spine, **19**(12), pp. 1310–1319.
[98] Holzapfel, G. A., Schulze-Bauer, C. A. J., Feigl, G., and Regitnig, P., 2004, "Single Lamellar Mechanics of the Human Lumbar Anulus Fibrosus," Biomech. Model. Mechanobiol., **3**(3), pp. 125–140.
[99] Stemper, B. D., Baisden, J. L., Yoganandan, N., Shender, B. S., and Maiman, D. J., 2014, "Mechanical Yield of the Lumbar Annulus: A Possible Contributor to Instability," J. Neurosurg.: Spine, **21**(4), pp. 608–613.
[100] Acaroglu, E. R., Iatridis, J. C., Setton, L. A., Foster, R. J., Mow, V. C., and Weidenbaum, M., 1995, "Degeneration and Aging Affect the Tensile Behavior of Human Lumbar Anulus Fibrosus," Spine, **20**(24), pp. 2690–2701.
[101] Best, B. A., Guilak, F., Setton, L. A., Zhu, W., Saed-Nejad, F., Ratcliffe, A., Weidenbaum, M., and Mow, V. C., 1994, "Compressive Mechanical Properties of the Human Anulus Fibrosus and Their Relationship to Biochemical Composition," Spine, **19**(2), pp. 212–221.
[102] Iatridis, J. C., Setton, L. A., Foster, R. J., Rawlins, B. A., Weidenbaum, M., and Mow, V. C., 1998, "Degeneration Affects the Anisotropic and Nonlinear Behaviors of Human Anulus Fibrosus in Compression," J. Biomech., **31**(6), pp. 535–544.
[103] Antoniou, J., Epure, L. M., Michalek, A. J., Grant, M. P., Iatridis, J. C., and Mwale, F., 2013, "Analysis of Quantitative Magnetic Resonance Imaging and Biomechanical Parameters on Human Discs With Different Grades of Degeneration," J. Magn. Reson. Imaging, **38**(6), pp. 1402–1414.
[104] Freeman, A. L., Buttermann, G. R., Beaubien, B. P., and Rochefort, W. E., 2013, "Compressive Properties of Fibrous Repair Tissue Compared to Nucleus and Annulus," J. Biomech., **46**(10), pp. 1714–1721.
[105] Iatridis, J. C., Kumar, S., Foster, R. J., Weidenbaum, M., and Mow, V. C., 1999, "Shear Mechanical Properties of Human Lumbar Annulus Fibrosus," J. Orthop. Res., **17**(5), pp. 732–737.
[106] Guerin, H. A. L., and Elliott, D. M., 2006, "Degeneration Affects the Fiber Reorientation of Human Annulus Fibrosus Under Tensile Load," J. Biomech., **39**(8), pp. 1410–1418.
[107] Fujita, Y., Wagner, D. R., Biviji, A. A., Duncan, N. A., and Lotz, J. C., 2000, "Anisotropic Shear Behavior of the Annulus Fibrosus: Effect of Harvest Site and Tissue Prestrain," Med. Eng. Phys., **22**(5), pp. 349–357.
[108] Wagner, D. R., and Lotz, J. C., 2004, "Theoretical Model and Experimental Results for the Nonlinear Elastic Behavior of Human Annulus Fibrosus," J. Orthop. Res., **22**(4), pp. 901–909.
[109] Green, T. P., Adams, M. A., and Dolan, P., 1993, "Tensile Properties of the Annulus Fibrosus II. Ultimate Tensile Strength and Fatigue Life," Eur. Spine J., **2**(4), pp. 209–214.
[110] Fujita, Y., Duncan, N. A., and Lotz, J. C., 1997, "Radial Tensile Properties of the Lumbar Annulus Fibrosus are Site and Degeneration Dependent," J. Orthop. Res., **15**(6), pp. 814–819.
[111] Sen, S., Jacobs, N. T., Boxberger, J. I., and Elliott, D. M., 2012, "Human Annulus Fibrosus Dynamic Tensile Modulus Increases With Degeneration," Mech. Mater., **44**, pp. 93–98.
[112] Cortes, D. H., Jacobs, N. T., DeLucca, J. F., and Elliott, D. M., 2014, "Elastic, Permeability and Swelling Properties of Human Intervertebral Disc Tissues: A Benchmark for Tissue Engineering," J. Biomech., **47**(9), pp. 2088–2094.
[113] Bron, J. L., van der Veen, A. J., Helder, M. N., van Royen, B. J., and Smit, T. H., 2010, "Biomechanical and In Vivo Evaluation of Experimental Closure Devices of the Annulus Fibrosus Designed for a Goat Nucleus Replacement Model," Eur. Spine J, **19**(8), pp. 1347–1355.
[114] Nerurkar, N. L., Elliott, D. M., and Mauck, R. L., 2007, "Mechanics of Oriented Electrospun Nanofibrous Scaffolds for Annulus Fibrosus Tissue Engineering," J. Orthop. Res., **25**(8), pp. 1018–1028.
[115] Nerurkar, N. L., Baker, B. M., Sen, S., Wible, E. E., Elliott, D. M., and Mauck, R. L., 2009, "Nanofibrous Biologic Laminates Replicate the Form and Function of the Annulus Fibrosus," Nat. Mater., **8**(12), pp. 986–992.
[116] Nerurkar, N. L., Han, W., Mauck, R. L., and Elliott, D. M., 2011, "Homologous Structure–Function Relationships Between Native Fibrocartilage and Tissue Engineered From MSC-Seeded Nanofibrous Scaffolds," Biomaterials, **32**(2), pp. 461–468.
[117] Nerurkar, N. L., Sen, S., Baker, B. M., Elliott, D. M., and Mauck, R. L., 2011, "Dynamic Culture Enhances Stem Cell Infiltration and Modulates Extracellular Matrix Production on Aligned Electrospun Nanofibrous Scaffolds," Acta Biomater., **7**(2), pp. 485–491.
[118] Koepsell, L., Remund, T., Bao, J., Neufeld, D., Fong, H., and Deng, Y., 2011, "Tissue Engineering of Annulus Fibrosus Using Electrospun Fibrous Scaffolds With Aligned Polycaprolactone Fibers," J. Biomed. Mater. Res., **99A**(4), pp. 564–575.
[119] Yeganegi, M., Kandel, R. A., and Santerre, J. P., 2010, "Characterization of a Biodegradable Electrospun Polyurethane Nanofiber Scaffold: Mechanical Properties and Cytotoxicity," Acta Biomater., **6**(10), pp. 3847–3855.
[120] Wismer, N., Grad, S., Fortunato, G., Ferguson, S. J., Alini, M., and Eglin, D., 2014, "Biodegradable Electrospun Scaffolds for Annulus Fibrosus Tissue Engineering: Effect of Scaffold Structure and Composition on Annulus Fibrosus Cells In Vitro," Tissue Eng., Part A, p. 140123085256009.
[121] Turner, K. G., Ahmed, N., Santerre, J. P., and Kandel, R. A., 2014, "Modulation of Annulus Fibrosus Cell Alignment and Function on Oriented Nanofibrous Polyurethane Scaffolds Under Tension," Spine J., **14**(3), pp. 424–434.
[122] Sharifi, S., van Kooten, T. G., Kranenburg, H.-J. C., Meij, B. P., Behl, M., Lendlein, A., and Grijpma, D. W., 2013, "An Annulus Fibrosus Closure Device Based on a Biodegradable Shape-Memory Polymer Network," Biomaterials, **34**(33), pp. 8105–8113.
[123] Vernengo, J., Fussell, G. W., Smith, N. G., and Lowman, A. M., 2010, "Synthesis and Characterization of Injectable Bioadhesive Hydrogels for Nucleus Pulposus Replacement and Repair of the Damaged Intervertebral Disc," J. Biomed. Mater. Res., **93B**(2), pp. 309–317.
[124] Cho, H., Park, S.-H., Park, K., Shim, J. W., Huang, J., Smith, R., Elder, S., Min, B.-H., and Hasty, K. A., 2013, "Construction of a Tissue-Engineered Annulus Fibrosus," Artif. Organs, **37**(7), pp. E131–E138.
[125] Martin, J. T., Milby, A. H., Chiaro, J. A., Kim, D. H., Hebela, N. M., Smith, L. J., Elliott, D. M., and Mauck, R. L., 2014, "Translation of an EngineeredNanofibrous Disc-Like Angle-Ply Structure for Intervertebral Disc Replacement in a Small Animal Model," Acta Biomater., **10**(6), pp. 2473–2481.
[126] Driscoll, T. P., Nerurkar, N. L., Jacobs, N. T., Elliott, D. M., and Mauck, R. L., 2011, "Fiber Angle and Aspect Ratio Influence the Shear Mechanics of Oriented Electrospun Nanofibrous Scaffolds," J. Mech. Behav. Biomed. Mater., **4**(8), pp. 1627–1636.
[127] Schek, R. M., Michalek, A. J., and Iatridis, J. C., 2011, "Genipin-Crosslinked Fibrin Hydrogels as a Potential Adhesive to Augment Intervertebral Disc Annulus Repair," Eur. Cell Mater., **21**, pp. 373–383.

[128] Guterl, C. C., Torre, O. M., Purmessur, D., Khyati, D., Likhitpanichkul, M., Hecht, A. C., Nicoll, S. B., and Iatridis, J. C., 2014, "Characterization of Mechanics and Cytocompatibility of Fibrin-Genipin Annulus Fibrosus Sealant With the Addition of Cell Adhesion Molecules," Tissue Eng. Part A, **20**(17–18), p. 140506130038007.
[129] Jeong, C. G., Francisco, A. T., Niu, Z., Mancino, R. L., Craig, S. L., and Setton, L. A., 2014, "Screening of Hyaluronic Acid–Poly(Ethylene Glycol) Composite Hydrogels to Support Intervertebral Disc Cell Biosynthesis Using Artificial Neural Network Analysis," Acta Biomater., **10**(8), pp. 3421–3430.
[130] Nerurkar, N. L., Mauck, R. L., and Elliott, D. M., 2008, "ISSLS Prize Winner: Integrating Theoretical and Experimental Methods for Functional Tissue Engineering of the Annulus Fibrosus," Spine, **33**(25), pp. 2691–2701.
[131] Wan, Y., Feng, G., Shen, F. H., Balian, G., Laurencin, C. T., and Li, X., 2007, "Novel Biodegradable Poly(1,8-octanediol malate) for Annulus Fibrosus Regeneration," Macromol. Biosci., **7**(11), pp. 1217–1224.
[132] Wiltsey, C., Christiani, T., Williams, J., Scaramazza, J., Van Sciver, C., Toomer, K., Sheehan, J., Branda, A., Nitzl, A., England, E., Kadlowec, J., Iftode, C., and Vernengo, J., 2015, "Thermogelling Bioadhesive Scaffolds for Intervertebral Disk Tissue Engineering: Preliminary In Vitro Comparison of Aldehyde-Based Versus Alginate Microparticle-Mediated Adhesion," Acta Biomater., **16**, pp. 71–80.
[133] Jiao, Y., Gyawali, D., Stark, J. M., Akcora, P., Nair, P., Tran, R. T., and Yang, J., 2012, "A Rheological Study of Biodegradable Injectable PEGMC/HA Composite Scaffolds," Soft Matter, **8**(5), pp. 1499–1507.
[134] Sitterle, V. B., Sun, W., and Levenston, M. E., 2008, "A Modified Lap Test to More Accurately Estimate Interfacial Shear Strength for Bonded Tissues," J. Biomech., **41**(15), pp. 3260–3264.
[135] Maher, S. A., Mauck, R. L., Rackwitz, L., and Tuan, R. S., 2010, "A Nano-Fibrous Cell Seeded Hydrogel Promotes Integration in a Cartilage Gap Model," J. Anat., **4**(1), pp. 25–29.
[136] Iatridis, J. C., and ap Gwynn, I., 2004, "Mechanisms for Mechanical Damage in the Intervertebral Disc Annulus Fibrosus," J. Biomech., **37**(8), pp. 1165–1175.
[137] Vergroesen, P.-P. A., Bochyn ska, A. I., Emanuel, K. S., Sharifi, S., Kingma, I., Grijpma, D. W., and Smit, T. H., 2015, "A Biodegradable Glue for Annulus Closure," Spine, **40**(9), pp. 622–628.
[138] Long, R. G., Buerki, A., Zysset, P., Eglin, D., Grijpma, D. W., Blanquer, S. B. G., Hecht, A. C., and Iatridis, J. C., 2015, "Mechanical Restoration and Failure Analyses of Composite Repair Strategy for Annulus Fibrosus," Acta Biomater., **30**, pp. 116–125.
[139] Gantenbein, B., Illien-Jünger, S., Chan, S., Walser, J., Haglund, L., Ferguson, S. J., Iatridis, J. C., and Grad, S., 2015, "Organ Culture Bioreactors-Platforms to Study Human Intervertebral Disc Degeneration and Regenerative Therapy," Curr. Stem Cell Res. Ther., **31**(23), pp. 339–352.
[140] Gawri, R., Mwale, F., Ouellet, J., Roughley, P. J., Steffen, T., Antoniou, J., and Haglund, L., 2011, "Development of an Organ Culture System for Long-Term Survival of the Intact Human Intervertebral Disc," Spine, **36**(22), pp. 1835–1842.
[141] Walter, B. A., Illien-Junger, S., Nasser, P. R., Hecht, A. C., and Iatridis, J. C., 2014, "Development and Validation of a Bioreactor System for Dynamic Loading and Mechanical Characterization of Whole Human Intervertebral Discs in Organ Culture," J. Biomech., **47**(9), pp. 2095–2101.
[142] Haglund, L., Moir, J., Beckman, L., Mulligan, K. R., Jim, B., Ouellet, J. A., Roughley, P., and Steffen, T., 2011, "Development of a Bioreactor for Axially Loaded Intervertebral Disc Organ Culture," Tissue Eng. Part C, **17**(10), pp. 1011–1019.
[143] O'Connell, G. D., Vresilovic, E. J., and Elliott, D. M., 2007, "Comparison of Animals Used in Disc Research to Human Lumbar Disc Geometry," Spine, **32**(3), pp. 328–333.
[144] Wang, S., Park, W. M., Kim, Y. H., Cha, T., Wood, K., and Li, G., 2014, "In Vivo Loads in the Lumbar L3–4 Disc During a Weight Lifting Extension," Clin. Biomech. (Bristol, Avon)., **29**(2), pp. 155–160.
[145] Michalek, A. J., Funabashi, K. L., and Iatridis, J. C., 2010, "Needle Puncture Injury of the Rat Intervertebral Disc Affects Torsional and Compressive Biomechanics Differently," Eur. Spine J., **19**(12), pp. 2110–2116.